CARDIFF UNIVERSITY
PRIFYSGOL CAERDYDD

ORCA – Online Research @ Cardiff

This is an Open Access document downloaded from ORCA, Cardiff University's institutional repository:https://orca.cardiff.ac.uk/id/eprint/161270/

This is the author's version of a work that was submitted to / accepted for publication.

Citation for final published version:

Chen, Yi-Ling, Ng, Jessica Soo Weei, Ottakandathil Babu, Rosana, Woo, Jeongmin, Nahler, Janina, Hardman, Clare S., Kurupati, Prathiba, Nussbaum, Lea, Gao, Fei, Dong, Tao, Ladell, Kristin , Price, David A. , Duncan, David A., Johnson, David, Gileadi, Uzi, Koohy, Hashem and Ogg, Graham S. 2023. Group A Streptococcus induces CD1a-autoreactive T cells and promotes psoriatic inflammation. Science Immunology 8 (84) , eadd9232. 10.1126/sciimmunol.add9232

Publishers page: http://dx.doi.org/10.1126/sciimmunol.add9232

Please note:
Changes made as a result of publishing processes such as copy-editing, formatting and page numbers may not be reflected in this version. For the definitive version of this publication, please refer to the published source. You are advised to consult the publisher's version if you wish to cite this paper.

This version is being made available in accordance with publisher policies. See http://orca.cf.ac.uk/policies.html for usage policies. Copyright and moral rights for publications made available in ORCA are retained by the copyright holders.

Group A Streptococcus induces CD1a-autoreactive T cells and promotes psoriatic inflammation

Yi-Ling Chen 1 , Jessica Soo Weei Ng 1 , Rosana Ottakandathil Babu 1 , Jeongmin Woo 1 , Janina Nahler 1 , Clare S. Hardman 1 , Prathiba Kurupati 1 , Lea Nussbaum 1 , Fei Gao 1,2, Tao Dong 1,2, Kristin Ladell 3 , David A. Price 3,4, David A. Duncan 5 , David Johnson 6 , Uzi Gileadi 1 , Hashem Koohy 1,7, Graham S. Ogg 1,2*

1 MRC Human Immunology Unit, MRC Weatherall Institute of Molecular Medicine, University of Oxford, Oxford, UK.
2 CAMS-Oxford International Centre for Translational Immunology, University of Oxford, Oxford, UK.
3 Division of Infection and Immunity, School of Medicine, Cardiff University, Cardiff, UK.
4 Systems Immunity Research Institute, School of Medicine, Cardiff University, Cardiff, UK.
5 Diamond Light Source, Harwell Science and Innovation Campus, Didcot, UK.
6 Department of Plastic and Reconstructive Surgery, John Radcliffe Hospital, Oxford University Hospitals National Health Services Foundation Trust, Oxford, UK.
7 Alan Turing Fellow in Health and Medicine, Oxford, UK.
*Corresponding author. Email: graham.ogg@ndm.ox.ac.uk

Group A Streptococcus (GAS) infection is associated with multiple clinical sequelae, including different subtypes of psoriasis. Such post-streptococcal disorders have been long known but are largely unexplained. CD1a is expressed at constitutively high levels by Langerhans cells and presents lipid antigens to T cells, but the potential relevance to GAS infection has not been studied. Here, we investigated whether GAS-responsive CD1a-restricted T cells contribute to the pathogenesis of psoriasis. Healthy individuals had high frequencies of circulating and cutaneous GAS-responsive CD4+ and CD8+ T cells with rapid effector functions, including the production of interleukin-22 (IL-22). Human skin and blood single-cell CITE-seq analyses of IL-22–producing T cells showed a type 17 signature with proliferative potential, whereas IFN-γ–producing T cells displayed cytotoxic T lymphocyte characteristics. Furthermore, individuals with psoriasis had significantly higher frequencies of circulating GAS-reactive T cells, enriched for markers of activation, cytolytic potential, and tissue association. In addition to responding to GAS, subsets of expanded GAS-reactive T cell clones/lines were found to be autoreactive, which included the recognition of the self-lipid antigen lysophosphatidylcholine. CD8+ T cell clones/lines produced cytolytic mediators and lysed infected CD1a-expressing cells. Furthermore, we established cutaneous models of GAS infection in a humanized CD1a transgenic mouse model and identified enhanced and prolonged local and systemic inflammation, with resolution through a psoriasis-like phenotype. Together, these findings link GAS infection to the CD1a pathway and show that GAS infection promotes the proliferation and activation of CD1a-autoreactive T cells, with relevance to post-streptococcal disease, including the pathogenesis and treatment of psoriasis.

INTRODUCTION

Psoriasis is a common inflammatory skin disease that carries significant morbidity and is associated with joint, intestinal, metabolic, and psychological disease (1). It has been long known that group A Streptococcus (GAS) throat infection can promote guttate psoriasis, but the underlying mechanisms have remained largely unexplained (2, 3). Laryngeal GAS and other subsets of β-hemolytic streptococcal infections often precede exacerbation of some forms of psoriasis, including plaque psoriasis (4, 5). Furthermore, tonsillectomy has been found to protect against plaque psoriasis, at least temporarily (6–8). Recurrent streptococcal throat infection is thought to be a form of immune susceptibility featuring antibody deficiency and impaired T follicular helper cell function, whereby streptococcal infection drives the expansion of skin-homing lymphocytes (9–11). Psoriasis risk is also

linked to individuals carrying the human leukocyte antigen (HLA)–Cw*0602 allele, and this has been widely assumed to be related to the presentation of peptides by HLA-Cw*0602 to T cells in the skin. It is known that HLA-Cw*0602 predisposes individuals to active streptococcal throat infection and that HLA-Cw6 can engage the inhibitory receptor KIR2DL1 (12, 13). Cw*0602 gene expression shows relative insensitivity to tumor necrosis factor–α (TNF-α)– and interferon-γ (IFN-γ)–mediated induction (14, 15), and an enhancer element of HLA-Cw*0602 is thought to explain the early onset of plaque psoriatic disease association (14). HLA-Cw*0602–positive individuals also benefit the most from the protective effect of tonsillectomy (7). Collectively, these findings are compatible with the hypothesis that impaired control of pharyngeal streptococcal infection drives a downstream non–major histocompatibility complex (non-MHC)–dependent cutaneous inflammatory response. The underlying pathways remain to be determined.

A number of mechanisms have been proposed to explain the link between GAS and psoriatic disease. T cell cross-reactivity between streptococcal M protein and skin keratins (e.g., keratin 17) has been described, but specific T cells are not present in psoriatic skin lesions (16–19). Furthermore, keratin 17 can be expressed at multiple different epithelia beyond the skin, including the proximal intestine, lung, and urogenital tract, which are not clinically involved during guttate psoriasis. Streptococcal superantigens have also been implicated in the pathogenesis of psoriasis, but the spatiotemporal relationship between streptococcal throat infection and guttate psoriasis is not fully compatible with such a mechanism; for example, guttate psoriasis typically arises 1 to 3 weeks after the onset of the throat infection rather than at the peak of throat symptoms (3, 20). Oligoclonal αβ T cell expansions have been described in lesional and resolved psoriatic skin, thought to be more in keeping with antigen-driven reactivity than broad superantigen effects (21). T cell responses to LL-37 and melanocyte ADAMTSL5 have also been described but have not yet been linked to streptococcal infection in the setting of psoriasis (22, 23). Overall, whereas these data confirm that a streptococcal-induced immune response can promote psoriatic inflammation, the specific pathways are yet to be fully explained.

CD1a is a relatively nonpolymorphic HLA class I–like molecule expressed at constitutively high levels by LCs (24). It can also be expressed by thymocytes and induced on dendritic cell subsets, T cells, and innate lymphoid cells (25, 26). CD1a presents endogenous and exogenous lipid antigens to T cells, inducing pro-inflammatory cytokines with relevance to psoriasis, including interleukin-22 (IL22), IL-17A, and IFN-γ (27–31). Elevated frequencies of CD1a-reactive T cells have been found in the blood and skin of patients with psoriasis, and imiquimod (IMQ)-induced inflammation is associated with exacerbated disease in a human CD1a transgenic mouse model (29, 32). T cell recognition of permissive skin lipid antigens can be mediated, at least in some cases, through T cell receptor (TCR) engagement of the A′ roof of CD1a without direct lipid:TCR contact, helping to explain broad lipid reactivity (33, 34). CD1a-reactive T cells have been shown to respond to mycobacterial and staphylococcal antigens, implicating a role in bacterial defense (24, 28, 35, 36). However, there are no studies that have investigated the role of CD1a reactivity in the immune response to GAS and the consequences for associated inflammatory disease. Here, we test the hypothesis that GAS induces CD1a reactivity and investigate the underlying mechanisms and relevance to psoriasis, with therapeutic implications.

RESULTS

Healthy individuals have high frequencies of circulating and cutaneous GAS-responsive CD1a-reactive T cells

To determine whether GAS-responsive CD1a-reactive T cells were present across a healthy cohort, we used CD1a-transfected K562 cells as target cells. K562 lacks HLA class I and II and mimics CD1a antigen presentation by primary antigen-presenting cells (29, 37, 38). K562-CD1a cells infected with GAS were recognized by ex vivo polyclonal T cells in a CD1a-dependent manner, leading to the production of IL-22 (Fig. 1A, left). All healthy adults tested had detectable GAS-responsive CD1a-reactive T cells, comprising a large population of circulating T cells (Fig. 1A, right). High frequencies of CD1a-reactive T cells have been predicted from in vitro expansions but not yet proven in ex vivo analyses (31, 39). The use of GAS as an antigen driver thus allowed the demonstration that CD1a-reactive T cells represent a large population of the circulating T cell repertoire and prompted our continued investigation of the nature of the T cell response.

Through gating on the IL-22–producing GAS-responsive T cells, we identified that this population comprised both CD4+ and CD8+ T cells, with slight enrichment of the CD4+ populations (Fig. 1B). They predominately expressed TCRαβ (Fig. 1C) and were enriched for CD45RO expression, consistent with previous antigen exposure (Fig. 1D) and existing findings (31, 39). As expected, the IL-22–producing GAS-responsive T cells were enriched for markers of T cell activation (Fig. 1E). These cells also had elevated expression of the skin-homing marker cutaneous lymphocyte-associated antigen (CLA), implicating a requirement for peripheral control of T cells that have the potential capacity to home to the skin (Fig. 1F).

Having identified a population of GAS-responsive T cells in healthy individuals, we went on to investigate their CD1a dependence and to test whether primary CD1a-expressing target cells could also mediate antigen presentation. Anti-CD1a blockade was able to effectively inhibit the recognition of GAS-infected K562- CD1a cells by IL-22–producing polyclonal ex vivo blood T cells (Fig. 2A), suggesting the possibility of therapeutic intervention in GAS-driven inflammatory skin disease. Heat-killed GAS was not able to induce a T cell response (Fig. 2B), suggesting a requirement for active K562-CD1a infection. These findings also rule out a role for heat-sensitive soluble mediators such as some TLR ligands. We next showed that both autologous monocyte-derived dendritic cells (mo-DCs) and Langerhans cell–like cells (LC-like DCs) were able to present GAS-associated antigensto polyclonal T cells in a CD1a-dependent manner (Fig. 2C). The blockade of MHC class I/II and CD1a was additive, suggesting that the pathways are acting in parallel to present peptide antigens and CD1a-dependent lipid-driven responses (26, 33, 38, 39). These data confirmed that ex vivo polyclonal IL-22–producing T cells were able to respond to primary CD1a-expressing cells infected with GAS. Only GAS was capable of inducing CD1a reactivity among the streptococcal and staphylococcal species tested (Fig. 2D). In addition, we were able to observe IFN-γ–producing CD1a-autoreactive T cell responses from healthy individuals, but no further net increase was observed after GAS infection (Fig. 2E). Furthermore, limited granulocyte-macrophage colony-stimulating factor (GM-CSF) or IL-17A–producing T cells were detected (Fig. 2E). These observations were further investigated in subsequent experiments. We next investigated whether GASresponsive CD1a-reactive T cells were present in healthy skin and found high frequencies of IL-22–producing cells in all individuals tested (Fig. 2F). Overall, the existence of a high frequency of GASresponsive CD1a-reactive T cells with rapid effector function is compatible with a requirement for these cells in defense against a ubiquitous and potentially lethal pathogen.

IL-22– and IFN-γ–secreting CD1a-reactive GAS-responsive T cells exhibit diverse functionalities

We next used single-cell analyses to test whether the T cells were enriched for particular subsets and whether they showed features of functional relevance, such as skin residence and activating/inhibitory receptor expression. A cellular indexing of transcriptomes and epitopes by sequencing (CITE-seq) dataset comprising GAS-responsive CD1a-reactive skin T cells was constructed using our previous K562-CD1a stimulation strategy to fluorescence-activated cell sorting (FACS) isolate IL-22– or IFN-γ–producing T cells. Non–IL22/IFN-γ–producing and ex vivo unstimulated skin T cells were included to establish a phenotypic baseline. We identified 15 phenotypically distinct clusters (Fig. 3A), with each cluster comprising cells from each donor (fig. S1, A and B). A degree of spatial separation was observed of T cells derived from each treatment condition (Fig. 3B and fig. S1C) and of CD4-expressing T helper cells(TH) and CD8-expressing T cytotoxic cells (Tc) (fig. S1D). Protein CD45RO, CD25, CD11a, and CD69 expressions were used to confirm that skin contains predominantly antigen-experienced T cell subsets (fig. S1, E and F).

CITE-seq antibodies against the fluorochromes phycoerythrin (PE) or allophycocyanin (APC) on the detection antibodies were included to further characterize IL-22– or IFN-γ–producing skin T cells, respectively. We observed a good association between mRNA and protein expression for IFN-γ (Fig. 3C), but IL-22 protein was expressed by more cellsthan IL22 RNA (Fig. 3D). Such discordancy is well described and may reflect protein/RNA analytical timing and emphasizes the importance of such RNA/protein multimodal analyses (40). Therefore, to capture all relevant populations, we grouped the CD1a-responding cells into five subgroups on the basis of their mRNA and protein (antibody-derived tag, ADT) expression of IL22 or IFN-γ: ADT–IL-22+ , RNA–IL-22+ , ADT–IFN-γ+ , RNA–IFNγ+ , and Neg (IL-22−IFN-γ−) (Fig. 3E). ADT–IL-22+ a 22+ T cells were enriched in clusters 1/2 and cluster 0, respectively, whereas ADT–IFN-γ+ and RNA–IFN-γ+ T cells were concentrated in clusters 4, 5, 8, and 9 (Fig. 3F and fig. S1G). In addition to IL-22 and IFN-γ, a small proportion of skin T cells could produce IL-17F, IL-10, IL-13, or IL-4 (Fig. 3G), indicating a broad spectrum of immune modulatory functions of CD1a-restricted T cells.

We found 480 differentially expressed genes (DEGs) and 501 DEGs that characterized each CD4+ and CD8+ subgroup, respectively (fig. S1H). IL-22–expressing CD4+ T cells also expressed TH17-associated cytokines [IL26, IL9, LTA (lymphotoxin-α), CSF2 (GM-CSF), and TNF (TNF-α)], core TH17 signature genes (RORC, CCR4, CCR6, IL4LI1, CTSH, IQCG, PXDC1, PPARG, and MSC) (41–44), as well as T cell activation–related genes [IL2RA, IL2RB, TNFRSF4 (OX40), ITGA4, CD40LG, and NME1], and metabolic, glycolytic, and oxidative stress response transcripts (TXN, PKM, HSP90AB1, and ENO1) (Fig. 3H). For example, thioredoxin (TRX), a small redox protein encoded by TXN, is induced by oxidative stressesto protect immune cells from apoptosis and promotes TH1 differentiation and IFN-γ production in T cells (45–47). Enolase 1, encoded by ENO1, is a critical regulator of the glycolytic and effector activity of CD8+ tumor-infiltrating lymphocytes (48). These cells also showed proliferation and cell adhesion capacity with increased expression of microtubules and cytoskeleton remodeling genes (TUBA1B, TUBB, TYMS, and MYO1G), membrane scaffolding and organization genes (VIM, BST2, LGALS3, and ADGRG1), and genes involved in oxidative phosphorylation, cholesterol, and fatty acid metabolism (COX5A, DUSP4, NDUFV2, FABP5, TMEM97, VDR, and HPGD) (Fig. 3H). ENO1, VDR (vitamin D receptor), and HPGD (hydroxyprostaglandin dehydrogenase) have been reported to facilitate the conversion of human CD4+ T cells into induced regulatory T (Treg), or to maintain Treg suppressive functions, suggesting a potentially acquired plasticity of these populations (49–51). The elevated gene profile was concentrated in the RNA–IL-22+ CD1a-restricted CD4+ T cells, but not in the ADT–IL-22+ population, implicating temporal regulatory mechanisms of gene expression in IL-22–producing T cells. IFNγ–producing CD4+ T cells displayed characteristics often associated with cytotoxic T lymphocytes (CTL), including high levels of inflammatory cytokines [IFNG, CSF1 (M-CSF), and CSF2

(GMCSF)], cytotoxic (GZMA, GZMH, PRF1, NKG7, and FASLG), chemotactic (CCL3, CCL4, CCL5, CXCR3, and CCR5), and transcription factor (TBX21 and Runx3) signatures, as well as being enriched for enzymes and inhibitors promoting cytolytic activity [CTSC (cathepsin C), CST7 (cystatin F), and APOBEC3G (cytidine deaminase)] (Fig. 3I). Several T cell exhaustion and inhibitory markers (PDCD1, LAG3, HAVCR2, and IL10) were also elevated in these CD4+ CTLs (Fig. 3I). Moreover, the majority of IFN-γ–producing CD8+ T cells exhibited elevated T cell cytotoxicity, migration, activation, survival, and exhaustion-related genes (Fig. 3J). This population displayed higher expression of MHC-II–related genes (HLADQA1, HLA-DQB1, HLA-DRB1, HLA-DRA, HLA-DPA1, HLADRB5, HLA-DPB1, and CD74) and genes related to cell cycling and division (CDK6, CCND2, TYMS, ZBTB32, and ADGRG1), suggestive of highly proliferating T cell phenotypes (Fig. 3J) (52).

We next identified differentially expressed immunophenotype markers for each CD1a-responding subgroup at the protein level. Each subgroup exhibited distinct molecular patterns which largely matched the RNA expression. CD1a-restricted CD4+ T cells expressed an array of activation markers [CD25 (IL2RA), CD71, OX40 (TNFRSF4), CD49d (ITGA4), and 4-1BB (TNFRSF9)], chemokine receptors related to CTL (CXCR3) and TH17, and inhibitory/exhaustion markers [PD-L1 (programmed death-ligand 1), PD-1 (programmed death-1) (PDCD1), LAG-3, and Tim3 (HAVCR2)] (Fig. 3K). Similar activating and inhibitory patterns were observed in CD1a-restricted CD8+ T cells, with the additional expression of natural killer cell receptor 2B4 and CD94, and chemokine receptor CCR5 (Fig. 3L). Consistent with the RNA results, HLA-DR was slightly elevated on IFN-γ–producing CD1a-reactive CD8+ T cells (Fig. 3L). Some IFN-γ–producing CD1a-reactive skin T cells displayed IL-2RB+ ITGAE+ CD69+ resident memory T cell (TR phenotypes (fig. S1I), indicating their roles in providing rapid tissue immune effector function. These results, together with the transcriptomic profiles observed, have characterized a diverse functionality of the IL-22– and IFN-γ–secreting CD1a-reactive CD4+ and CD8+ T cells.

To understand the differentiation signatures of CD1a-reactive T cells, we constructed single-cell trajectories using the Monocle 3 R package (53); small clusters (with cell number <165) 13, 14, and 15 were removed and the remaining T cells were placed on the pseudo time trajectories based on changes in the transcriptome (Fig.4A and fig. $2), with unstimulated T Cells assigned as the root node for ordering . The majority of unstimulated T cells and CD1a-GAS Neg (IL-22−IFN-γ−) population distributed throughout the early pseudo-time, whereas most of the IL-22– and IFN-γ–producing subgroups were found in later pseudo-timie, showing a clear temporal separation (Fig. 4, B to D). We inspected the transition of expression values along the pseudo-time for previously established genes associated with CD1a-restricted T cell activation and found their expression to correlate with the temporal development of T cell activation and differentiation. We identified a gradual increase in the expression of genes encoding chemotactic and cytotoxic molecules, as well as concordant expression of migration, inhibition, and proliferation molecules, matching the progressive differentiation states of T cell effector functions (Fig. 4E and fig. S2B). After the separation of CD4+ and CD8+ subsets, both CD4+ CTLs and CD8+ CTLs were found to be distributed in the latter half of the pseudo-time (Fig. 4E), showing a convergent differentiation CD4+ and CD8+ T cells. Several genes were also found to be down-regulated rapidly during the course of T cell activation, including genes essential for the homeostatic survival of naive T cells, such as PIK3IP1, GIMAP7, and IL-7R (fig. S2C). Similar patterns of T cell activation were also observed on surface protein marker expression (Fig. 4F). The data confirm that during activation, CD1a-reactive T cells follow a similar pattern of gene expression that has been observed for peptide-specific T cells, emphasizing an adaptive-like pathway in response to stimulation. Last, we examined CDR3 residue composition using GLIPH2 software (54) to detect potential conserved CDR3 motifs with CD1a specificity. Expanded TCR clonotypes from cells located

at early and late pseudo-time were searched for enriched CDR3 motifs, and multiple CDR3α, but not CDR3β, motif candidates were identified within these T cell populations. The percentage of T cells containing those motifs, for both CD4+ and CD8+ populations, are shown in Fig. 4, G and H, respectively, showing differed motif preference in CD1a-reactive T cells located at late pseudo-time. In summary, we describe a comprehensive phenotype of CD1a-reactive T cells during stimulation and show coordinated expression of activation and differentiation markers.

Patients with psoriasis have elevated frequencies and activation of GAS-reactive T cells

We and others have previously shown that patients with psoriasis exhibit aberrant release of type 22 and 17 related cytokines upon pan-T stimuli (fig. S3) (55), as well as elevated circulating and cutaneous CD1a-reactive T cells (29, 32), but there have been no studies that have addressed the relevance of GAS in the CD1a pathway in patients. Given that we have demonstrated here that GAS can drive a CD1a-autoreactive effector T cell response, we next tested whether individuals with plaque psoriasis have altered frequencies and phenotypes of GAS-responsive T cells. Patients with psoriasis had significantly elevated frequencies of IL-22–producing circulating GAS-responsive CD1a-reactive T cells (Fig. 5A). CD1a-autoreactive and GAS-responsive CD1a-reactive blood T cells producing IL-22 or IFN-γ from five healthy and three psoriatic individuals were subjected to multiomic analysis, and 19 clusters of T cell subsets and states were identified after Uniform Manifold Approximation and Projection (UMAP) visualization (Fig. 5B), with cluster enrichment of T cells derived from each treatment condition as observed in the skin dataset (Fig. 5C). In blood T cells, IL-22 RNA expression level was only detected in 11 cells; hence, we relied on both the RNA/protein expression and the sorting strategy of IL22–producing populations to group the CD1a-responding cells into three subgroups: IL-22+ , IFN-γ+ , and Neg (IL-22−IFN-γ−). IFN-γ–producing T cells generally formed distinct clusters from IL-22–producing cells, and, as expected, whereas CD1a-autoreactive cells comprised both IL-22 and IFN-γ–producing cells, CD1a-GAS–reactive cells were predominantly IL-22 secreting (Fig. 5D). Both naive and antigen-experienced T cell subsets were found in the circulation (fig. S4A).

Blood IFN-γ– or IL-22–producing CD1a-reactive T cells shared similar gene expression patterns to skin CD1a-reactive T cells. In short, CD1a-autoreactive and GAS-reactive CD4+ and CD8+ T cells were highly active and proliferative, expressing genes related to T cell effector functions, cytoskeleton remodeling, cell adhesion, and metabolic programming (Fig. 5, E and F, and fig. S4B). T cells with a naive phenotype equipped with the capacity of producing multiple cytokines (TCNP cells) have been described in human and mouse models (56, 57). Here, we observed that naive blood T cells, concentrated in clusters 10 and 16, showed the ability to respond to CD1a presentation (Fig. 5D and fig. S4A). As opposed to the skin, some CD4+ IL-22–producing CD1a-reactive blood T cells, instead of displaying a TH17 phenotype, exhibited abilities to produce TH1 and cytolytic functionality (Fig. 5, E and F), suggesting potential plasticity among blood TH subsets in response to the inflammatory milieu.

Next, we compared the phenotypes of IFN-γ–producing or IL22–producing CD1a-reactive T cells from healthy and psoriatic individuals. The main DEGs were found within the CD4+ T cell population (Fig. 5, G and H). To highlight, psoriatic CD1a-reactive T cells displayed higher characteristics of cytotoxicity, with elevated expression of genes playing a role in the formation of secretory granules (SGRN), and genes linked to their killing potential [ITGB1 (CD29)] (Fig. 5I) (58, 59), as well as transcription factors involved in TCR signaling (FOS and JUN) (60) and components in the TCR signaling cascade, including calcium-binding/signaling proteins S100A11, S100A4, S100A6, and

AHNAK and costimulatory molecules CD82 and CD63 (Fig. 5I). Furthermore, several of the transcripts encoding proteins with established roles in T cell chemotaxis, adhesion, tissue trafficking (CXCR4, CD99, ITGB7, LGALS1, LGALS3, KLRB1, and AQP3), as well as cell division and proliferation (PASK, TAGLN2, MYO1F, MYO1G, TMSB4X, and MT2A), were also higher in psoriatic CD1a-reactive T cells (Fig. 5J). KLF6, which has been reported to strongly associate with T cell activation in psoriasis, was also found to be expressed at higher levels in CD1a-GAS reactive IL-22–producing T cells (fig. S4C) (61). The hyperactive phenotype of psoriatic CD1a-reactive T cells was confirmed in surface protein profiles showing upregulated activation markers CD25 and CD69, expression of tissueassociated markers CCR5 and CD161 (KLRB1), and inhibitory markers Tim3 and PD-1(Fig. 5, K and L). Overall, these data show that individuals with psoriasis have higher frequencies of activated GAS-responsive CD1a-reactive T cells.

GAS drives the activation of CD1a-reactive T cells

To investigate the underlying mechanisms, we sorted IL-22–producing GAS-reactive T cells using flow cytometry and went on to successfully establish T cell clones/lines derived from blood and skin. The blood and skin clones/lines were able to recognize GAS-infected K562-CD1a cells (Fig. 6A), and this could be inhibited by anti-CD1a blockade (Fig. 6B). The isolated clones/lines were unable to show enhanced recognition of K562-CD1a infected with other streptococcal and staphylococcal species with importance to the skin and other epithelial barrier surfaces, suggesting that the CD1a pathway is particularly relevant to S. pyogenes of those tested (fig. S5, A and B). Clones/lines could be either CD4+ or CD8+ , but all maintained their ability to produce IL-22 in response to GAS-infected K562-CD1a cells. Some T cell clones/lines could also recognize uninfected K562-CD1a cells, suggesting their potential CD1a autoreactivity, and this was explored next.

CD8+ GAS-reactive T cells lyse infected and uninfected target cells

Given the single-cell ex vivo data showing evidence of cytolytic potential within the GAS-reactive CD8+ T cells, we next tested whether the CD8+ subset had a cytolytic function. Streptococcus is known to bind to LCs and can infect mononuclear phagocytic cells and epithelial cells (62–64). We first confirmed the mRNA signal observed in the ex vivo single-cell analysis and showed the production of TNF-α, granzyme A (GZMA), and granzyme B (GZMB) at the protein level in response to GAS-infected target cells (Fig. 6, C and D). Furthermore, the clones/lines were able to lyse GAS-infected target cells, implicating a role of the CD8+ T cells in the death of infected cells (Fig. 6E and fig. S6). The CD8+ T cell clones/lines could also recognize uninfected K562-CD1a target cells (Fig. 6, C to E) and produce high quantities of GM-CSF, granulysin, and perforin (Fig. 6F). These data show that many GAS-reactive CD8+ T cells can lyse CD1a-expressing GAS-infected target cells but can also show autoreactivity, with implications for effector function at uninfected sites and mechanisms underlying immunopathology of post-streptococcal disease. Given the autoreactivity of the GASdriven T cells, we next explored candidate self-lipid antigens for recognition by this subpopulation of T cells.

A proportion of GAS-reactive T cells can respond to the selflipid lysophosphatidylcholine

We have previously shown that endogenous and exogenous phospholipases (PLA2) can generate lipid antigens for recognition by CD1a-reactive T cells (29, 37, 38). Furthermore, the PLA2 lipid products lysophosphatidylcholine (LPC) and oleic acid are known permissive CD1a ligands (34, 38). It is of interest that S. pyogenes expresses PLA2 activity that participates in host-pathogen interaction and is a virulence factor (65, 66). Here, we show that a proportion of the GAS-driven T cell clones/lines recognize LPC-pulsed K562-CD1a cells (Fig. 6, G to H). These data suggest that GAS infection is in part detected by recognition of self-lipid antigens, which are products of the PLA2 pathway.

Recent advances in CD1a tetramer technology facilitate the identification of CD1a-reactive T cells recognizing specific lipids (36, 67). To detect the frequency of CD1a-LPC–reactive T cells in individuals with plaque psoriasis, we next tetramerized CD1a monomers treated with CHAPS detergent (mock) or different species of LPCs (fig. S7A) and stained polyclonal blood T cells. A significantly higher frequency ex vivo of circulating CD1a-LPC tetramer– binding T cells (Fig. 6I and fig. S7, B and C) was identified in these patients, in line with our finding of elevated GAS-reactive CD1a-restricted effector T cell responses in patients with psoriasis (Fig. 5). Overall, the data suggest that GAS can drive the activation of CD1aautoreactive T cells that can respond to skin stress lipids, including LPC, implicating their involvement in psoriatic immunopathology.

It was noted that not all the GAS-driven T cells recognized K562- CD1a cells in the absence of GAS, so it is likely that there are other bacterial-specific ligands recognized by other GAS-reactive T cells. Therefore, whereas the IFN-γ–producing CD1a-reactive T cell frequency was not altered in net ex vivo polyclonal T cells in response to GAS infection (Fig. 2E), we tested whether this might mask individual patterns of GAS reactivity at the clonal T cell level. We sorted and clonally expanded IFN-γ–producing CD1a-autoreactive T cell lines from blood. Unexpectedly, about half of the IFN-γ–producing CD1a-autoreactive T cell lines recognized GAS-pulsed K562-CD1a cells (Fig. 6J, left), whereas the autoreactivity of other T cell lines was inhibited by GAS-derived ligands (Fig. 6J, right), which supports the possibility of other bacterial-specific CD1a ligands generated during GAS infection. Overall, these data identify permissive self-lipid LPCs as a potential target for subsets of GAS reactive T cells.

CD1a reactivity is TCR dependent

To address the TCR-mediated CD1a reactivity, we sequenced the TCRs of three GAS-responsive CD1a-autoreactive T cell clones (3G2, 1D8, and 3G4) and undertook TCR gene transfer experiments using CRISPR-Cas9 editing to orthotopically replace endogenous TCRs with target TCRs via homology-directed repair (HDR). T cells engineered with the transgenic TCRs were isolated and expanded (Fig. 7, A and B) and were able to bind to CD1a-mock (detergent-treated CD1a) and CD1a-LPC tetramers (Fig. 7, C to F), as well as recognize CD1a-expressing K562 cells (Fig. 7G) or bead bound CD1a proteins treated with CHAPS detergent (mock) (Fig. 7H). Moreover, when TCR-transgenic T cells were cocultured with bead-bound CD1a protein streated with synthetic LPC species, further increases in cytokine production were detected (Fig. 7I), suggesting that the T cells could respond to CD1a that was enhanced in the presence of the permissive ligand LPC. Furthermore, the engineered T cells were able to recognize GAS-infected K562- CD1a cells in a CD1a-dependent manner (Fig. 7J). Together, the data show that the CD1a reactivity of the T cell clones is TCR dependent and confirms reactivity to mock CD1a and enhanced with the CD1a loaded with the self-lipid LPC.

GAS infection drives a CD1a-dependent psoriasis-like inflammatory response in vivo

CD1a presents both endogenous and exogenous lipid antigens to activate T cells in human CD1a transgenic (CD1a-Tg) challenge models, including the sensitization of mice skin with urushiol, a sap compound found in poison ivy, and IMQ, a TLR7 agonist that can trigger psoriasiform inflammation (32, 68). To investigate whether GAS can exacerbate skin inflammation through CD1a in vivo, we intradermally challenged CD1a-Tg and wild-type (WT) mice with live GAS to the ear skin, and the skin inflammation was assessed at days 1 and 8 after infection (Fig. 8A). Ear thickness was significantly increased after GAS infection and advanced further in the presence of CD1a (Fig. 8B). The appearance of a typical lesion progression after GAS infection showed marked erythema and scaling and expanded lesion sites in the CD1a-Tg mice (Fig. 8C). Histological analysis revealed an increased thickening of both the epidermis and dermis of GAS-infected CD1a-Tg mice compared with those of

WT mice, with increased rete ridge prominence, both of which are known features of psoriatic inflammation (Fig. 8D). Confocal fluorescence microscopy analysis of skin showed the infiltration of CD1a-expressing cells and their proximity to GAS, suggesting the near-neighbour potential of antigen processing and presentation (Fig. 8E).

We analyzed the skin, draining lymph node, and spleen cells by flow cytometry and found a significant increase in lymphocytes, neutrophils, and monocytes after GAS infection, but the relative proportions of the immune cells were not significantly different between WT and CD1a-Tg mice (fig. S8). However, the presence of CD1a promoted the production of IL-22 and IFN-γ from both CD4+ and CD8+ draining lymph node T cells after GAS infection (Fig. 8, F and G). Cytokine profile analysis of skin extracts also showed an overall inflammatory myeloid-related cytokine up-regulation after GAS infection (fig. S9); we observed an increased concentration of IL-23, which plays an essential role in type 17 pathway induction in psoriasis, at day 1, and elevated IFN-γ levels at day 8 (Fig. 8H).

We next investigated the longitudinal effects of GAS infection in CD1a-Tg mice using a distal application of the IMQ model (68). We subcutaneously challenged CD1a-Tg and WT mice with live GAS to the back, and after GAS clearance (day 14), daily topical skin application of IMQ cream on the distal ear skin induced significant psoriasiform inflammation (Fig. 8, I and J). CD1a-Tg mice with prior GAS infection displayed more pronounced pathological changes of scaliness, erythema, and significantly increased ear thickness (Fig. 8, J and K). An increase in IL-17A–producing T cells in the ear skin of the CD1a-Tg mice was identified in GAS-experienced CD1a-Tg mice (Fig. 8L). In addition, T cells derived from skin draining lymph nodes and spleens of IMQ/GAS-treated CD1a-Tg mice exhibited enhanced responsiveness to CD1a presentation in vitro (fig. S10). Collectively, the mouse in vivo models have provided evidence of a role of GAS in driving psoriatic skin inflammation, which is enhanced in the presence of CD1a.

DISCUSSION

Post-streptococcal inflammatory disease has long been known in the clinic, but the mechanisms underlying pathogenesis have not been fully elucidated. Here, we have shown that GAS-responsive CD1a-reactive T cells comprise a substantial portion of the human αβ T cell repertoire, accounting for up to 5 to 10% of T cells. Subsets of the CD1a-reactive cells, which activate and proliferate in response to GAS, can also respond to the self-lipid antigen LPC, a known PLA2 product present in the skin. This suggests that GAS can drive a CD1a-dependent autoreactive T cell response, allowing LPC to act as a signal of tissue damage in response to bacterial infection.

In contrast to common pharyngeal intracellular presence, group A streptococci are detected at low levels in healthy and psoriatic skin and blood (69, 70). Given published literature and the data shown here, during active GAS pharyngeal infection, it is likely that CD1a autoreactive T cells will proliferate, activate, and acquire skinhoming receptor expression. Therefore, through mounting a local tissue response, it is conceivable that GAS will have the potential to drive ensuing CD1a-dependent cutaneous inflammation.

CD1a-reactive T cells were found to produce IL-22, which is known to be elevated in psoriatic skin lesions, and serum levels correlate with disease activity (71). Furthermore, IL-22 can promote keratinocyte proliferation and production of antimicrobial responses (71, 72). It is of interest that IL-22 is also elevated in wounds, a psoriasis lesions can show the Koebner phenomenon, where disease develops at sites of skin trauma. LPC is produced during platelet activation at wounds, and elevated levels of LPC are detectable in lesional psoriatic skin (73). In addition, CD1a is expressed by large

numbers of infiltrating dendritic cell populations infiltrating skin wounds (25, 74, 75). It is therefore possible that a similar mechanism could contribute to forms of sterile inflammation such as the Koebner phenomenon.

It was noted that many of the CD1a-autoreactive T cells were CD8+ and had cytolytic activity. These cells may have the capacity to kill infected cells in vivo, reducing the intracellular GAS reservoir within CD1a-expressing cells. Intracellular residence is known to provide an advantage to GAS, because there is relative protection from neutrophil degranulation, antibody- and complement-mediated inhibition, and some antibiotic effects (76). ACD1a-dependent mechanism of killing would provide the immune system with an alternative strategy for bacterial reservoir control that would depend less on relatively inefficient cross-presentation pathways. However, it was also noted that the CD8+ T cells could lyse uninfected CD1a-expressing targets, confirming that bacterial-driven T cell reactivity can drive a CD1a-dependent autoreactive response and associated inflammation.

On the basis of our current understanding of MHC-peptide recognition by T cells, it might be predicted that there would be diverse lipid antigens for recognition. Whereas this is likely to be true, the data suggest that, under inflammatory conditions, subsets of the GAS-responsive CD1a reactive T cells can recognize broad families of permissive self-lipids, of which LPC was studied here. These data and published data (33) challenge the exquisite antigen-specific discrimination accepted within MHC-peptide dogma, where under inflammatory conditions, the diverse GAS-responsive CD1a-reactive T cells can be co-opted to control GAS infection through recognition of skin self-lipids. Such a system must be tightly controlled, which may include spatial separation, inhibitory receptor and inhibitory lipid expression (67), and the nature of the local inflammatory milieu. It is likely that other layers of local control will be deployed, including a role for regulatory T cells. Nevertheless, it is clear that many of the CD1a-reactive T cells that are induced by GAS infection can respond to the self-lipid LPC and drive autoreactivity.

By linking GAS infection to the CD1a pathway, the data presented point to a wider interpretation of post-streptococcal disease in which GAS drives autoimmunity across different tissues. Whereas this may be mediated through differential pathways at different sites, the findings identify nonpeptide self-ligands to be of broader relevance and extend the Gell and Coombs classification that implicates a requirement for the haptenation of nonpeptide ligands. Given that CD1a is relatively nonpolymorphic, this raises the possibility that broadly applicable therapeutics targeting CD1a may be feasible. Psoriasis is very common, affecting up to 2% of the population, suggesting that there may be selection advantages, perhaps related to cutaneous immunity. The findings presented here would be compatible with the possibility that the GAS induced CD1a-autoreactive T cells contribute to the GAS-specific immune response but at a cost of increased risk of psoriatic disease. This has relevance not only for understanding fundamental biology related to bacterial-associated inflammation but also in terms of capitalizing on a therapeutic window before the inflammatory sequelae ensure.

MATERIALS AND METHODS

Study design

The objective of this study was to determine the involvement of the CD1a pathway in the pathogenesis relevance of post-streptococcal sequelae. We assessed the frequencies and functionalities of the CD1a-restrictive GAS response circulating and cutaneous T cells from healthy individuals or patients with psoriasis, using singlecell CITE-seq, T cell clonal expansion, and orthotopic TCR replacement. Randomization was not required because of the lack of intervention,

and blinded assessment of results was not performed. Clinic participants were only excluded if they were on systemic immunosuppression. Inter-donor variation of functional responses was expected, because of the age, gender, ethnicity, and medical history of the individual recruited. Transgenic mice were used for in vivo GAS infection experiments, with approved humane endpoints. Animals were age-matched and randomly assigned, and the studies were unblinded. The number of samples/donors/ animals and the number of independent experiments are indicated in the figure legends. The sample size was determined on the basis of previous studies (25, 29, 37, 68).

Cell lines

Empty vector–transfected K562 (K562-EV) and CD1a-transfected K562 (K562-CD1a) cells (a gift from B. Moody, Brigham and Womens Hospital, Harvard Medical School, Boston, MA) were maintained in R10 [RPMI 1640 medium supplemented with 10% fetal calf serum (FCS), penicillin (100 IU/ml), streptomycin (100 μg/ml) (Gibco), 2 mM L-glutamine (Gibco), 1× nonessential amino acids (NEAAs) (Gibco), 1 mM sodium pyruvate (Gibco), 10 mM Hepes (Gibco), and 50 μM 2-mercaptoethanol (Gibco)], and G418 antibiotic (800 μg/ml) (Thermo Fisher Scientific).

Bacterial strains and culture conditions

S. pyogenes (GAS) serotype M18 strain (American Type Culture Collection, BAA572TM) was collected in the United States in 1987. The following reagent was obtained through the National Institutes of Health (NIH) Biodefense and Emerging Infections Research Resources Repository, NIAID, NIH as part of the Human Microbiome Project: Staphylococcus epidermidis (Strain BCM0060; HM-140), Streptococcus mitis (Strain F0392; HM-262), and Streptococcus pneumoniae (Strain TCH8431; HM-145). All bacteria strains were preserved in 10% glycerol stock and stored at −80°C. The frozen bacteria strains were streaked onto Columbia horse blood agar plates (OXOID) and cultured overnight at 37°C in a humidified 5% CO2 incubator. Colonies were collected and resuspended in Dulbecco's phosphate-buffered saline (DPBS) (no calcium, no magnesium) before their use in infection experiments. To obtain bacteria culture at the log phase of growth, bacteria were grown in Todd-Hewitt broth (Sigma-Aldrich) overnight in 5% CO2 at 37°C without shaking. The culture was pelleted by spinning at 2500 rpm and resuspended in DPBS (no calcium, no magnesium). Heat-killed bacteria were generated by incubating the bacteria at 65°C for 10 min.

Isolation of human blood and skin T cells

Human blood samples were obtained from healthy participants or individuals with plaque psoriasis, and skin samples were obtained from healthy donors undergoing plastic surgery. The individuals with psoriasis did not have arthritis and were not on systemic therapy. All specimens were taken under good clinical practice guidance with ethical approval (14/SC/0106, National Research Ethics Service). Clinical metadata of psoriasis patients are shown in table S1. Peripheral blood mononuclear cells (PBMCs) were isolated using Lymphoprep (Stem Cell Technologies) gradient isolation. Skin samples were dissected and incubated with collagenase P (1 mg/ml; Roche) overnight at 37°C with 5% CO2. The next day, deoxyribonuclease (DNase) I (100 μg/ml; Roche Diagnostic) was added for 15 to 30 min. Cold 10 mM EDTA solution was then added to the sample to stop the digestion. The digested tissue was passed through a 70-μm cell strainers, and mononuclear cells were harvested with Lymphoprep gradient isolation before further procedures. Blood and skin T cells were isolated using magnetic-activated cell sorting with CD3 MicroBeads (Miltenyi Biotec) following the manufacturer's protocol and resting in T cell medium (TCM) [RPMI 1640 medium supplied with 10% human serum (HS), penicillin (100 IU/ml), streptomycin (100 μg/ml; Gibco), 2 mM L-glutamine (Gibco), 1× NEAAs (Gibco), 1 mM sodium pyruvate (Gibco), 10 mM Hepes (Gibco), 50 μM 2-mercaptoethanol (Gibco)] and IL-2 (200 IU/ml; BioLegend) for 72 hours.

Secretion assay

K562-EV or K562-CD1a cells were pulsed with GAS (multiplicity of infection = 50 or 100) for 72 hours, and the extracellular bacteria were removed before coculturing with T cells. In some conditions, K562-EV or K562-CD1a cells were pulsed with LPC 18:1 (150 μM; Avanti Polar Lipids) for 16 hours, and the excess lipids were removed before coculturing with T cells. Blood or skin T cells (1 × 106) were cocultured with control/pulsed K562-EV or K562- CD1a (0.5 × 106) cells for 4 to 6 hours. In indicated conditions, K562-CD1a was pretreated with anti-CD1a blocking antibody (10 μg/ml) or immunoglobulin G1 (IgG1) isotype control (10 μg/ml; BioLegend) for 1 hour before the addition of T cells. Cytokine-producing responder T cells were detected using Cytokine Secretion Assays (Miltenyi Biotec) following the manufacturer's instructions. T cells were coated with anti-cytokine (IL-22, IFN-γ, GM-CSF, or IL-17A) antibodies after coculture to detect CD1a-dependent autocrine cytokine production using fluorochrome-conjugated detection antibodies. Antibodies against surface markers identify T cells (anti-CD3, anti-CD4, anti-CD8, and anti-TCRαβ) and their phenotypes (anti-CD45RA, anti-CD45RO, anti-CD25, anti-CD69, anti-CD137, anti-CD154, and anti-CLA). Data were acquired using an LSRFortessa X-50 flow cytometer (BD Biosciences) and further analyzed with FlowJo (FlowJo LLC) software.

Sample preparation, CITE-seq staining, and single-cell RNA-seq

Skin T cells from four healthy individuals and blood T cells from five healthy and three psoriatic (plaque psoriasis) donors were subjected to single-cell multiomic analysis. To construct a dataset comprising GAS-responsive CD1a-reactive T cells, we adapted our previous K562-CD1a stimulation strategy. PE- or APC-conjugated detection antibodies were used to detect IL-22– or IFN-γ–producing T cells, respectively. After the FACS antibodies staining step of the T cell secretion assay, cells were incubated with FcX block (BioLegend) for 10 min and stained with TotalSeq-C antibody pool (table S2) and a unique hashtag for each sample at 4°C for 30 min. Cells were then washed three times in staining buffer (0.4% bovine serum albumin in PBS) and filtered using a 40-μm Flowmi filter (Sigma-Aldrich) and pooled in equal proportions. IL-22–producing, IFN-γ–producing, and non–IL-22/IFN-γ–producing T cells after coculture with K562-CD1a or GAS-infected K562-CD1a cells were sorted. Ex vivo isolated unstimulated T cells were included to establish a phenotypic baseline. Cells were loaded into nine lanes of two 10X Genomics Chip G, at 20,000 to 30,000 cells per lane using a Chromium Single Cell Controller (10X Genomics, Pleasanton, CA) with the Chromium Single Cell 5' Library and Gel Bead Kit v1.1. The remaining steps were carried out according to the manufacturer's instructions, and Cell Surface Protein/Immune Receptor Mapping Libraries and 5' Gene Expression (GEX) Libraries were generated. Final libraries were sequenced on a NovoSeq 6000 (Illumina, San Diego) to achieve an average depth of 5000 raw reads per cell for CITE-seq Libraries and 25,000 raw reads per cell for GEX Libraries.

Data processing, alignment, quality control, and hashtag demultiplexing of single-cell RNA-seq

For each sequenced single-cell RNA sequencing (scRNA-seq) pool, CellRanger toolkit (version 6.0.1; 10X Genomics; https://support. 10xgenomics.com/single-cell-gene-expression/software/ downloads/latest) was used to process raw data, map cDNA libraries against hg38 human reference genome from the UCSC ftp site (77), and summarize unique molecular identifier (UMI) counts against the corresponding Ensemble gene annotations (78). The hashed feature count matrix was CLR (centered log-ratio)–normalized and demultiplexed on the basis of their sample of origin using the R package Seurat's HTOdemux function. Briefly, normalized counts for each hash ID were fitted with a negative binomial distribution. A positive threshold was set to the 99th percentile of the recovered normalized UMI counts for the hashtag, where cells below this threshold were considered negative for the tag. Cells negative for hashtags and cells positive for multiple hashtags were filtered out. After

filtering out and assigning the cells of origin on the basis of HTO staining, we further removed the cells with fewer than 200 or greater than 4000 detected genes and less than 1% or greater than 10% mitochondrial reads per each library. With 13 mitochondrial and 104 ribosomal genes that were highly variable among samples, genes that were expressed in <10 cells were removed from the final count matrix. The total number of UMI count per dell, percentage of mitochondrial features, and individual donor effects were regressed out during the library merging. In total, 14,732 sequenced skin effector T cells and 15,176 blood T cells passed quality control, doublet exclusion, and removal of FOXP3-expressing populations. Further details can be found in supplementary Material and Methods.

CD1a-reactive T cell clone/line generation and activation analysis

CD1a-restricted T cells were isolated by FACS after coculture with noninfected/infected K562-EV or K562-CD1a cells. The live responder cells were then single-cell–sorted into a 96-well Ubottom culture plate and expanded with a mixed lymphocyte reaction. The expanded T cell clones/lines were then checked for purity and CD1a responsiveness using Cytokine Secretion Assays (Miltenyi Biotec). Briefly, noninfected/infected K562-EV/CD1a (2 × 105) cells were cocultured with 1 × 105 to 5 × 105 CD1a-reactive T cell lines/clones for 4 hours with the addition of helper cytokines to support CD1a-dependent cytokine production: IL-12 (1 ng/ml; BioLegend), IL-18 (1 ng/ml; BioLegend) and IL-2 (25 U/ml; BioLegend) for IFN-γ–producing T cells, and IL-6 (5 ng/ml; BioLegend), TNF-α (5 ng/ml; BioLegend), and IL-2 (25 U/ml; BioLegend) for IL-22–producing T cell culture. The supernatant was collected and stored at −80°C.

FACS-based cytotoxicity assay

Target K562-EV/CD1a cells were fluorescently labeled with Cell Trace Violet (Invitrogen) before the infection. CD1a-restricted T cell lines/clones (1 × 105 to 5 × 105) were added to noninfected/infected target K562-EV/CD1a cells (2 × 105) in the presence of IL-12 (1 ng/ml; BioLegend) and IL-18 (1 ng/ml; BioLegend) and IL-2 (25 U/ml; BioLegend). The supernatant was collected after 24-hour coculture for cytokine analysis. Cell death was assessed by flow cytometry after 48-hour coculture. Briefly, the wells were harvested, and to stain for dead and apoptotic cells, Zombie Fixable Viability dyes (1:1000; BioLegend) and annexin V–APC (BioLegend) were added. To allow quantitative analysis of the target cell populations, 2 × 105 carboxyfluorescein diacetate succinimidyl ester–labeled K562 cells (as reference cells) were added. This was done just before the FACS analysis to avoid the interaction between the target, reference, and T cells. Data were acquired using an LSRFortessa X-50 flow cytometer (BD Biosciences) and further analyzed with FlowJo (FlowJo LLC) software. The percentage of induced killing was then calculated with the following equation by comparing the frequency of live target and reference populations: % cytotoxicity = 100 − ((% live target cells /% live reference cells)/(% live cells of untreated K562-EV/% live reference cells) × 100).

CD1a tetramer staining

Biotinylated human CD1a monomers (NIH Tetramer Core Facility) were produced in human embryonic kidney 293–derived cell lines (36, 67). CD1a (10 μg) was treated with a 100X molar excess of LPC 18:1 or LPC 18:0 (Avanti Polar Lipids) in tris-buffered saline containing 0.25% CHAPS or vehicle alone (mock) for 16 hours at 37°C and tetramerized with PE-streptavidin (High Concentration; BioLegend) at a molar ratio of 5:1. T cells (<1x10 6) were washed twice in FACS staining buffer (BioLegend) at room temperature and stained with 0.5 μl of tetramerin 20 μl of FACS staining buffer at 37°C for 30 min with gentle shaking. Anti-CD3 antibody (OKT3; 0.1 μg in 10 μl; BioLegend) was added to the cells and incubated for an additional 10 min at 37°C with gentle shaking. Tetramers and anti-CD3 antibody were removed before staining surface markers CD3 (UCHT1; BioLegend), CD4,

CD8, and Zombie Fixable Viability dyes (BioLegend) for 15 min at 4°C. Cells were washed once and resuspended in FACS buffer and ready for requisition using an LSRFortessa X-50 flow cytometer (BD Biosciences) and further analyzed with FlowJo (FlowJo LLC) software.

HDR DNA template design

DNA templates were designed in silico, synthesized by GeneArt, and presented in pMK vectors (Life Technologies, Thermo Fisher Scientific). The structure of the HDR template was designed following the previously published method (79). The full lengths of the α and β chains of the TCR to be introduced, self-cleaving peptides P2 to ensure the separation of both TCR chains, and a poly-A tail (bGHpA) were flanked by left and right homology arms. Both α and β chains consist of the human variable regions and the murine constant region with an additional disulfide bond (80) to facilitate the identification of re-expressed transgenic TCR with anti-mouse TCRβ antibody.

Cas9 RNP production

CRISPR-Cas9 single-guide RNA (sgRNA) (Integrated DNA Technologies) composed of both CRISPR RNA (crRNA) and trans-activating crRNA (tracrRNA) sequences were used. sgRNAs targeting both TRBC1 and TRBC2 (5′-GGAGAATGACGAGTGGACCC-3′) (81) and TRAC (5′-AGAGTCTCTCAGCTGGTACA-3′) (82) were mixed with Alt-R S.p.Cas9 Nuclease V3 (Integrated DNA Technologies) at a 3:1 molar ratio and incubated for 15 min at room temperature.

Orthotopic TCR replacement in primary human T cells

Frozen PBMCs were thawed and rested at 2 × 106 to 3 × 106 cells per ml in TCM containing IL-2 (50 U/ml; BioLegend) and IL-15 (5 ng/ ml; BioLegend) overnight at 37°C, 5% CO2. PBMCs then were activated for 2 days with anti-human CD3/CD28 magnetic Dynabeads (Thermo Fisher Scientific) at a beads-to-cells ratio of 1:1 in IL-2– (200 U/ml; BioLegend) and IL-15–supplemented (5 ng/ml; BioLegend) TCM. Activated PBMC cells (5 to 10 × 106) were harvested and electroporated with ribonucleoprotein mixture and HDR DNA templates (2.5 μg) using a P3 Primary Cell 4D-Nucleofector X Kit S (Lonza) and a 4D Nucleofector X unit (Lonza) using the EO115 electroporation program following the manufacturer's protocol. Electroporated cells were seeded into a 24-well plate at a density of 5 × 106 to 10 × 106 cells per ml in TCM containing IL-2 (200 U/ml; BioLegend). Mouse TCRβ-expressing T cells were sorted 3 to 5 days after electroporation and expanded with a mixed lymphocyte reaction. The expanded TCR-transgenic T cells were subjected to subsequent functional assays. When coculturing with K562-EV/ CD1a or GAS-infected K562-EV/CD1a cells for 4 hours, expanded TCR-transgenic T cells were supplied with IL-6 (5 ng/ml; BioLegend), TNF-α (5 ng/ml; BioLegend), IL-2 (25 U/ml; BioLegend), and anti-CD3 (OKT3; 5 ng/ml; BioLegend) or IL-12 (1 ng/ml; BioLegend), IL-18 (1 ng/ml; BioLegend), and IL-2 (25 U/ml; BioLegend) to support CD1a-dependent cytokine production.

Mice

Mice were bred and maintained under specific pathogen–free conditions at University of Oxford, and all experiments were conducted in accordance with the approval of the UK Home Office. CD1a transgenic C57BL/6 mice (CD1a-Tg) were generated in Oxford and have been previously described (68), and age-matched WT littermates were used as controls. Six to 10 weeks of age male and female mice were used for experiments and randomized into the different conditions.

Skin challenge model

WT and CD1a-Tg mice were anesthetized by isoflurane inhalation and were treated intradermally with either 10 μl of PBS or GAS (2 × 106) in PBS to the dorsal side of the ear pinnae. Alternatively,

WT and CD1a-Tg mice were anesthetized by isoflurane inhalation and were treated subcutaneously with either 20 µl of PBS or GAS (4 × 106) in PBS to the shaved back. Fourteen days after initial GAS challenges, 25 mg of Aldara cream containing 5% IMQ was applied to the dorsal and ventral sides of the ear pinnae daily for 6 days. Ear thickness was measured before and after challenges using a micrometer scale on indicated days, and photos of the challenge sites were documented. Mice were euthanized, and ears, draining lymph nodes, spleen, and blood were harvested for flow cytometry, histological, and cytokine/chemokine profile analyses.

Mouse tissue processing

Ears were dissected into small pieces and digested in 500 µl of RPMI 1640 containing 10% FCS and collagenase P (1 mg/ml; Roche Diagnostic) for an initial 1 hour at 37°C. The digested tissues were briefly spun at 2000 rpm for 5 min, and the 200 µl of clear supernatant were collected and stored at −20°C for LEGENDplex analysis. The remaining tissue pellets were resuspended thoroughly with another 1 ml of RPMI 1640 + collagenase P for another 1-hour incubation at 37°C, and DNase I (100 µg/ml; Roche Diagnostic) was added for the final 30 min. The digested samples were passed through 70-µm cell strainers (BD Biosciences), and the digestion was stopped with 500 µl of cold 10 mM EDTA in PBS, and a single-cell suspension was obtained in FACS cell staining buffer (BioLegend). Auricular lymph nodes were harvested and meshed through 70-µm cell strainers (BD Biosciences) to obtain singlecell suspensions in FACS cell staining buffer (BioLegend).

Statistical analysis

Data are presented as means ± SEM. Some results were calculated as the fold change of each condition to indicated control. Two-tailed paired/unpaired t test and one and two-way analysis of variance (ANOVA) tests were performed using GraphPad Prism version 9.00 (GraphPad Software).

REFERENCES AND NOTES

1. C. E. M. Griffiths, A. W. Armstrong, J. E. Gudjonsson, J. Barker, Psoriasis. Lancet 397, 1301–1315 (2021).
2. H. J. Whyte, R. D. Baughman, Acute guttate psoriasis and streptococcal infection. Arch. Dermatol. 89, 350–356 (1964).
3. D. Y. Leung, J. B. Travers, R. Giorno, D. A. Norris, R. Skinner, J. Aelion, L. V. Kazemi, M. H. Kim, A. E. Trumble, M. Kotb et al., Evidence for a streptococcal superantigen-driven process in acute guttate psoriasis. J. Clin. Invest. 96, 2106–2112 (1995).
4. J. E. Gudjonsson, A. M. Thorarinsson, B. Sigurgeirsson, K. G. Kristinsson, H. Valdimarsson, Streptococcal throat infections and exacerbation of chronic plaque psoriasis: A prospective study. Br. J. Dermatol. 149, 530–534 (2003).
5. R. H. Thorleifsdottir, J. H. Eysteinsdottir, J. H. Olafsson, M. I. Sigurdsson, A. Johnston, H. Valdimarsson, B. Sigurgeirsson, Throat infections are associated with exacerbation in a substantial proportion of patients with chronic plaque psoriasis. Acta Derm. Venereol. 96, 788–791 (2016).
6. R. H. Thorleifsdottir, S. L. Sigurdardottir, B. Sigurgeirsson, J. H. Olafsson, M. I. Sigurdsson, H. Petersen, S. Arnadottir, J. E. Gudjonsson, A. Johnston, H. Valdimarsson, Improvement of psoriasis after tonsillectomy is associated with a decrease in the frequency of circulating T cells that recognize streptococcal determinants and homologous skin determinants. J. Immunol. 188, 5160–5165 (2012). 7. R. H. Thorleifsdottir, S. L. Sigurdardottir, B. Sigurgeirsson, J. H. Olafsson, H. Petersen, M. I. Sigurdsson,J. E. Gudjonsson, A. Johnston, H. Valdimarsson, HLA-Cw6 homozygosity in plaque psoriasis is associated with streptococcal throat infections and pronounced improvement after tonsillectomy: A prospective case series. J. Am. Acad. Dermatol. 75, 889–896 (2016).
8. R. H. Thorleifsdottir, S. L. Sigurdardottir, B. Sigurgeirsson, J. H. Olafsson, M. I. Sigurdsson, H. Petersen, J. E. Gudjonsson, A. Johnston, H. Valdimarsson, Patient-reported outcomes and clinical response in patients with

moderate-to-severe plaque psoriasis treated with tonsillectomy: A randomized controlled trial. Acta Derm. Venereol. 97, 340–345 (2017).
9. J. M. Dan, C. Havenar-Daughton, K. Kendric, R. Al-Kolla, K. Kaushik, S. L. Rosales, E. L. Anderson, C. N. LaRock, P. Vijayanand, G. Seumois, D. Layfield, R. I. Cutress, C. H. Ottensmeier, C. S. Lindestam Arlehamn, A. Sette, V. Nizet, M. Bothwell, M. Brigger, S. Crotty, Recurrent group A Streptococcus tonsillitis is an immunosusceptibility disease involving antibody deficiency and aberrant TFH cells. Sci. Transl. Med. 11, eaau3776 (2019).
10. Y. Seong, N. H. Lazarus, L. Sutherland, A. Habtezion, T. Abramson, X. S. He, H. B. Greenberg, E. C. Butcher, Trafficking receptor signatures define blood plasmablasts responding to tissue-specific immune challenge. JCI Insight 2, e90233 (2017).
11. S. L. Sigurdardottir, R. H. Thorleifsdottir, H. Valdimarsson, A. Johnston, The association of sore throat and psoriasis might be explained by histologically distinctive tonsils and increased expression of skin-homing molecules by tonsil T cells. Clin. Exp. Immunol. 174, 139–151 (2013).
12. L. Mallbris, K. Wolk, F. Sanchez, M. Stahle, HLA-Cw*0602 associates with a twofold higher prevalence of positive streptococcal throat swab at the onset of psoriasis: A case control study. BMC Dermatol. 9, 5 (2009).
13. M. Vales-Gomez, R. A. Erskine, M. P. Deacon, J. L. Strominger, H. T. Reyburn, The role of zinc in the binding of killer cell Ig-like receptors to class I MHC proteins. Proc. Natl. Acad. Sci. U.S.A. 98, 1734–1739 (2001).
14. A. Clop, A. Bertoni, S. L. Spain, M. A. Simpson, V. Pullabhatla, R. Tonda, C. Hundhausen, P. Di Meglio, P. De Jong, A. C. Hayday, F. O. Nestle, J. N. Barker, R. J. Bell, F. Capon, R. C. Trembath, An in-depth characterization of the major psoriasissusceptibility locusidentifies candidate susceptibility alleles within an HLA-C enhancer element. PLOS ONE 8, e71690 (2013).
15. C. Hundhausen, A. Bertoni, R. K. Mak, E. Botti, P. Di Meglio, A. Clop, U. Laggner, S. Chimenti, A. C. Hayday, J. N. Barker, R. C. Trembath, F. Capon, F. O. Nestle, Allele-specific cytokine responses at the HLA-C locus: Implications for psoriasis. J. Invest. Dermatol. 132, 635–641 (2012).
16. A. S. Gudmundsdottir, H. Sigmundsdottir, B. Sigurgeirsson, M. F. Good, H. Valdimarsson, I. Jonsdottir, Is an epitope on keratin 17 a major target for autoreactive T lymphocytes in psoriasis? Clin. Exp. Immunol. 117, 580–586 (1999).
17. B. S. Baker, D. W. Brown, V. A. Fischetti, J. M. Ovigne, W. Porter, A. Powles, L. Fry, Skin T cell proliferative response to M protein and other cell wall and membrane proteins of group A streptococci in chronic plaque psoriasis. Clin. Exp. Immunol. 124, 516–521 (2001).
18. Z. Shen, L. Chen, Y. F. Liu, T. W. Gao, G. Wang, X. L. Fan, J. Y. Fan, P. S. Fan, C. Y. Li, B. Liu, Y. P. Dang, C. X. Li, Altered keratin 17 peptide ligands inhibit in vitro proliferation of keratinocytes and T cells isolated from patients with psoriasis. J. Am. Acad. Dermatol. 54, 992–1002 (2006).
19. H. Valdimarsson, R. H. Thorleifsdottir, S. L. Sigurdardottir, J. E. Gudjonsson, A. Johnston, Psoriasis–as an autoimmune disease caused by molecular mimicry. Trends Immunol. 30, 494–501 (2009).
20. L. Nahary, A. Tamarkin, N. Kayam, S. Sela, L. Fry, B. Baker, A. Powles, S. Rogers, I. Benhar, An investigation of antistreptococcal antibody responses in guttate psoriasis. Arch. Dermatol. Res. 300, 441–449 (2008).
21. T. R. Matos, J. T. O'Malley, E. L. Lowry, D. Hamm, I. R. Kirsch, H. S. Robins, T. S. Kupper, J. G. Krueger, R. A. Clark, Clinically resolved psoriatic lesions contain psoriasis-specific IL17-producing αβ T cell clones. J. Clin. Invest. 127, 4031–4041 (2017).
22. R. Lande, E. Botti, C. Jandus, D. Dojcinovic, G. Fanelli, C. Conrad, G. Chamilos, L. Feldmeyer, B. Marinari, S. Chon, L. Vence, V. Riccieri, P. Guillaume, A. A. Navarini, P. Romero, A. Costanzo, E. Piccolella, M. Gilliet, L. Frasca, The antimicrobial peptide LL37 is a T-cell autoantigen in psoriasis. Nat. Commun. 5, 5621 (2014).
23. A. Arakawa, K. Siewert, J. Stohr, P. Besgen, S. M. Kim, G. Ruhl, J. Nickel, S. Vollmer, P. Thomas, S. Krebs, S. Pinkert, M. Spannagl, K. Held, C. Kammerbauer, R. Besch, K. Dornmair, J. C. Prinz, Melanocyte antigen triggers autoimmunity in human psoriasis. J. Exp. Med. 212, 2203–2212 (2015). 24. R. E. Hunger, P. A. Sieling, M. T. Ochoa, M. Sugaya, A. E. Burdick, T. H. Rea, P. J. Brennan, J. T. Belisle, A. Blauvelt, S. A. Porcelli, R. L. Modlin, Langerhans cells utilize CD1a and langerin to efficiently present nonpeptide antigens to T cells. J. Clin. Invest. 113, 701–708 (2004).
25. Y. L. Chen, T. Gomes, C. S. Hardman, F. A. Vieira Braga, D. Gutowska-Owsiak, M. Salimi, N. Gray, D. A. Duncan, G. Reynolds, D. Johnson, M. Salio, V. Cerundolo, J. L. Barlow, A. N. J. McKenzie, S. A. Teichmann, M. Haniffa, G. Ogg, Re-evaluation of human BDCA-2+ DC during acute sterile skin inflammation. J. Exp. Med. 217, (2020).

26. C. S. Hardman, Y. L. Chen, M. Salimi, R. Jarrett, D. Johnson, V. J. Jarvinen, R. J. Owens, E. Repapi, D. J. Cousins, J. L. Barlow, A. N. J. McKenzie, G. Ogg, CD1a presentation of endogenous antigens by group 2 innate lymphoid cells. Sci. Immunol. 2, eaan5918 (2017).
27. S. Porcelli, M. B. Brenner, J. L. Greenstein, S. P. Balk, C. Terhorst, P. A. Bleicher, Recognition of cluster of differentiation 1 antigens by human CD4-CD8-cytolytic T lymphocytes. Nature 341, 447–450 (1989).
28. D. B. Moody, D. C. Young, T. Y. Cheng, J. P. Rosat, C. Roura-Mir, P. B. O'Connor, D. M. Zajonc, A. Walz, M. J. Miller, S. B. Levery, I. A. Wilson, C. E. Costello, M. B. Brenner, T cell activation by lipopeptide antigens. Science 303, 527–531 (2004).
29. K. L. Cheung, R. Jarrett, S. Subramaniam, M. Salimi, D. Gutowska-Owsiak, Y. L. Chen, C. Hardman, L. Xue, V. Cerundolo, G. Ogg, Psoriatic T cells recognize neolipid antigens generated by mast cell phospholipase delivered by exosomes and presented by CD1a. J. Exp. Med. 213, 2399–2412 (2016). 30. A. de Jong, T. Y. Cheng, S. Huang, S. Gras, R. W. Birkinshaw, A. G. Kasmar, I. Van Rhijn, V. PenaCruz, D. T. Ruan, J. D. Altman, J. Rossjohn, D. B. Moody, CD1a-autoreactive T cells recognize natural skin oils that function as headless antigens. Nat. Immunol. 15, 177–185 (2014).
31. A. de Jong, V. Pena-Cruz, T. Y. Cheng, R. A. Clark, I. Van Rhijn, D. B. Moody, CD1a-autoreactive T cells are a normal component of the human αβ T cell repertoire. Nat. Immunol. 11, 1102–1109 (2010).
32. J. H. Kim, Y. Hu, T. Yongqing, J. Kim, V. A. Hughes, J. Le Nours, E. A. Marquez, A. W. Purcell, Q. Wan, M. Sugita, J. Rossjohn, F. Winau, CD1a on Langerhans cells controls inflammatory skin disease. Nat. Immunol. 17, 1159–1166 (2016).
33. R. N. Cotton, T. Y. Cheng, M. Wegrecki, J. Le Nours, D. P. Orgill, B. Pomahac, S. G. Talbot, R. A. Willis, J. D. Altman, A. de Jong, G. Ogg, I. Van Rhijn, J. Rossjohn, R. A. Clark, D. B. Moody, Human skin is colonized by T cells that recognize CD1a independently of lipid. J. Clin. Invest. 131, e140706 (2021). 34. R. W. Birkinshaw, D. G. Pellicci, T. Y. Cheng, A. N. Keller, M. Sandoval-Romero, S. Gras, A. de Jong, A. P. Uldrich, D. B. Moody, D. I. Godfrey, J. Rossjohn, αβ T cell antigen receptor recognition of CD1a presenting self lipid ligands. Nat. Immunol. 16, 258–266 (2015).
35. A. T. Dang, R. M. Teles, P. T. Liu, A. Choi, A. Legaspi, E. N. Sarno, M. T. Ochoa, K. Parvatiyar, G. Cheng, M. Gilliet, B. R. Bloom, R. L. Modlin, Autophagy links antimicrobial activity with antigen presentation in Langerhans cells. JCI Insight 4, e126955 (2019).
36. G. C. Monnot, M. Wegrecki, T. Y. Cheng, Y. L. Chen, B. N. Sallee, R. Chakravarthy, I. M. Karantza, S. Y. Tin, A. E. Khaleel, I. Monga, L. N. Uwakwe, A. Tillman, B. Cheng, S. Youssef, S. W. Ng, A. Shahine, J. A. Garcia-Vilas, A. C. Uhlemann, L. A. Bordone, A. Han, C. H. Rohde, G. Ogg, D. B. Moody, J. Rossjohn, A. de Jong, Staphylococcal phosphatidylglycerol antigens activate human T cells via CD1a. Nat. Immunol. 24, 110–122 (2023).
37. R. Jarrett, M. Salio, A. Lloyd-Lavery, S. Subramaniam, E. Bourgeois, C. Archer, K. L. Cheung, C. Hardman, D. Chandler, M. Salimi, D. Gutowska-Owsiak, J. B. de la Serna, P. G. Fallon, H. Jolin, A. McKenzie, A. Dziembowski, E. I. Podobas, W. Bal, D. Johnson, D. B. Moody, V. Cerundolo, G. Ogg, Filaggrin inhibits generation of CD1a neolipid antigens by house dust mite-derived phospholipase. Sci. Transl. Med. 8, 325ra18 (2016).
38. E. A. Bourgeois, S. Subramaniam, T. Y. Cheng, A. De Jong, E. Layre, D. Ly, M. Salimi, A. Legaspi, R. L. Modlin, M. Salio, V. Cerundolo, D. B. Moody, G. Ogg, Bee venom processes human skin lipids for presentation by CD1a. J. Exp. Med. 212, 149–163 (2015).
39. C. de Lalla, M. Lepore, F. M. Piccolo, A. Rinaldi, A. Scelfo, C. Garavaglia, L. Mori, G. De Libero, P. Dellabona, G. Casorati, High-frequency and adaptive-like dynamics of human CD1 selfreactive T cells. Eur. J. Immunol. 41, 602–610 (2011).
40. M. Stoeckius, C. Hafemeister, W. Stephenson, B. Houck-Loomis, P. K. Chattopadhyay, H. Swerdlow, R. Satija, P. Smibert, Simultaneous epitope and transcriptome measurement in single cells. Nat. Methods 14, 865–868 (2017).
41. D. Hu, S. Notarbartolo, T. Croonenborghs, B. Patel, R. Cialic, T. H. Yang, D. Aschenbrenner, K. M. Andersson, M. Gattorno, M. Pham, P. Kivisakk, I. V. Pierre, Y. Lee, K. Kiani, M. Bokarewa, E. Tjon, N. Pochet, F. Sallusto, V. K. Kuchroo, H. L. Weiner, Transcriptional signature of human pro-inflammatory T(H)17 cells identifies reduced IL10 gene expression in multiple sclerosis. Nat. Commun. 8, 1600 (2017).
42. M. L. Puiffe, A. Dupont, N. Sako, J. Gatineau, J. L. Cohen, D. Mestivier, A. Lebon, A. PrevostBlondel, F. Castellano, V. Molinier-Frenkel, IL4I1 accelerates the expansion of effector CD8(+) T cells at the expense of memory precursors by increasing the threshold of T-cell activation. Front. Immunol. 11, 600012 (2020).

43. G. Castro, X. Liu, K. Ngo, A. De Leon-Tabaldo, S. Zhao, R. Luna-Roman, J. Yu, T. Cao, R. Kuhn, P. Wilkinson, K. Herman, M. I. Nelen, J. Blevitt, X. Xue, A. Fourie, W. P. Fung-Leung, RORγt and RORα signature genes in human TH17 cells. PLOS ONE 12, e0181868 (2017).
44. V. S. Wacleche, J. P. Goulet, A. Gosselin, P. Monteiro, H. Soudeyns, R. Fromentin, M. A. Jenabian, S. Vartanian, S. G. Deeks, N. Chomont, J. P. Routy, P. Ancuta, New insights into the heterogeneity of TH17 subsets contributing to HIV-1 persistence during antiretroviral therapy. Retrovirology 13, 59 (2016).
45. M. W. Kang, J. Y. Jang, J. Y. Choi, S. H. Kim, J. Oh, B. S. Cho, C. E. Lee, Induction of IFN-gamma gene expression by thioredoxin: Positive feed-back regulation of Th1 response by thioredoxin and IFN-gamma. Cell. Physiol. Biochem. 21, 215–224 (2008).
46. S. H. Kim, J. Oh, J. Y. Choi, J. Y. Jang, M. W. Kang, C. E. Lee, Identification of human thioredoxin as a novel IFN-gamma-induced factor: Mechanism of induction and its role in cytokine production. BMC Immunol. 9, 64 (2008).
47. H. Tian, Y. Matsuo, A. Fukunaga, R. Ono, C. Nishigori, J. Yodoi, Thioredoxin ameliorates cutaneous inflammation by regulating the epithelial production and release of pro-inflammatory cytokines. Front. Immunol. 4, 269 (2013).
48. L. F. Gemta, P. J. Siska, M. E. Nelson, X. Gao, X. Liu, J. W. Locasale, H. Yagita, C. L. Slingluff Jr., K. L. Hoehn, J. C. Rathmell, T. N. J. Bullock, Impaired enolase 1 glycolytic activity restrains effector functions of tumor-infiltrating CD8+ T cells. Sci. Immunol. 4, eaap9520 (2019).
49. V. De Rosa, M. Galgani, A. Porcellini, A. Colamatteo, M. Santopaolo, C. Zuchegna, A. Romano, S. De Simone, C. Procaccini, C. La Rocca, P. B. Carrieri, G. T. Maniscalco, M. Salvetti, M. C. Buscarinu, A. Franzese, E. Mozzillo, A. La Cava, G. Matarese, Glycolysis controlsthe induction of human regulatory T cells by modulating the expression of FOXP3 exon 2 splicing variants. Nat. Immunol. 16, 1174–1184 (2015).
50. D. Lu, B. Lan, Z. Din, H. Chen, G. Chen, Avitamin D receptor agonist converts CD4+ T cellsto Foxp3+ regulatory T cells in patients with ulcerative colitis. Oncotarget 8, 53552–53562 (2017).
51. A. Sharma, D. Rudra, Emerging functions of regulatory T Cells in tissue homeostasis. Front. Immunol. 9, 883 (2018).
52. S. Simon, V. Voillet, V. Vignard, Z. Wu, C. Dabrowski, N. Jouand, T. Beauvais, A. Khammari, C. Braudeau, R. Josien, O. Adotevi, C. Laheurte, F. Aubin, C. Nardin, S. Rulli, R. Gottardo, N. Ramchurren, M. Cheever, S. P. Fling, C. D. Church, P. Nghiem, B. Dreno, S. R. Riddell, N. Labarriere, PD-1 and TIGIT coexpression identifies a circulating CD8 T cell subset predictive of response to anti-PD-1 therapy. J. Immunother. Cancer 8, e001631 (2020).
53. J. Cao, M. Spielmann, X. Qiu, X. Huang, D. M. Ibrahim, A. J. Hill, F. Zhang, S. Mundlos, L. Christiansen, F. J. Steemers, C. Trapnell, J. Shendure, The single-cell transcriptional landscape of mammalian organogenesis. Nature 566, 496–502 (2019).
54. H. Huang, C. Wang, F. Rubelt, T. J. Scriba, M. M. Davis, Analyzing the Mycobacterium tuberculosis immune response by T-cell receptor clustering with GLIPH2 and genome-wide antigen screening. Nat. Biotechnol. 38, 1194–1202 (2020). 55. Y. Deng, C. Chang, Q. Lu, The inflammatory response in psoriasis: A comprehensive review. Clin Rev Allergy Immunol 50, 377–389 (2016).
56. M. P. Hosking, C. T. Flynn, J. L. Whitton, Antigen-specific naive CD8+ T cells produce a single pulse of IFN-γ in vivo within hours of infection, but without antiviral effect. J. Immunol. 193, 1873–1885 (2014).
57. V. Orlando, M. P. La Manna, D. Goletti, F. Palmieri, E. Lo Presti, S. A. Joosten, C. La Mendola, S. Buccheri, T. H. M. Ottenhoff, F. Dieli, N. Caccamo, Human CD4 T-cells with a naive phenotype produce multiple cytokines during Mycobacterium tuberculosis infection and correlate with active disease. Front. Immunol. 9, 1119 (2018).
58. B. P. Nicolet, A. Guislain, F. P. J. van Alphen, R. Gomez-Eerland, T. N. M. Schumacher, M. van den Biggelaar, M. C. Wolkers, CD29 identifies IFN-γ–producing human CD8+ T cells with an increased cytotoxic potential. Proc. Natl. Acad. Sci. U.S.A. 117, 6686–6696 (2020).
59. B. P. Nicolet, A. Guislain, M. C. Wolkers, CD29 enriches for cytotoxic human CD4(+) T cells. J. Immunol. 207, 2966–2975 (2021).
60. A. G. Papavassiliou, A. M. Musti, The multifaceted output of c-Jun biological activity: Focus at the junction of CD8 T cell activation and exhaustion. Cell 9, 2470 (2020).
61. N. Palau, A. Julia, C. Ferrandiz, L. Puig, E. Fonseca, E. Fernandez, M. Lopez-Lasanta, R. Tortosa, S. Marsal, Genome-wide transcriptional analysis of T cell activation reveals differential gene expression associated with psoriasis. BMC Genomics 14, 825 (2013).

62. W. P. Reed, C. Metzler, E. Albright, Streptococcal adherence to Langerhans cells: A possible step in the pathogenesis of streptococcal pharyngitis. Clin. Immunol. Immunopathol. 70, 28–31 (1994).
63. T. G. Loof, M. Rohde, G. S. Chhatwal, S. Jung, E. Medina, The contribution of dendritic cells to host defenses against Streptococcus pyogenes. J Infect Dis 196, 1794–1803 (2007).
64. F. Jendoubi, M. Rohde, J. C. Prinz, Intracellular streptococcal uptake and persistence: A potential cause of erysipelas recurrence. Front. Med. 6, 6 (2019).
65. M. J. Nagiec, B. Lei, S. K. Parker, M. L. Vasil, M. Matsumoto, R. M. Ireland, S. B. Beres, N. P. Hoe, J. M. Musser, Analysis of a novel prophage-encoded group A Streptococcus extracellular phospholipase A(2). J. Biol. Chem. 279, 45909–45918 (2004).
66. M. Oda, H. Domon, M. Kurosawa, T. Isono, T. Maekawa, M. Yamaguchi, S. Kawabata, Y. Terao, Streptococcus pyogenes phospholipase A(2) induces the expression of adhesion molecules on human umbilical vein endothelial cells and aorta of mice. Front. Cell. Infect. Microbiol. 7, 300 (2017).
67. R. N. Cotton, M. Wegrecki, T. Y. Cheng, Y. L. Chen, N. Veerapen, J. Le Nours, D. P. Orgill, B. Pomahac, S. G. Talbot, R. Willis, J. D. Altman, A. de Jong, I. Van Rhijn, R. A. Clark, G. S. Besra,
G. Ogg, J. Rossjohn, D. B. Moody, CD1a selectively captures endogenous cellular lipidsthat broadly block T cell response. J. Exp. Med. 218, e20202699 (2021).
68. C. S. Hardman, Y. L. Chen, M. Wegrecki, S. W. Ng, R. Murren, D. Mangat, J. P. Silva, R. Munro, W. Y. Chan, V. O'Dowd, C. Doyle, P. Mori, A. Popplewell, J. Rossjohn, D. Lightwood, G. S. Ogg, CD1a promotes systemic manifestations of skin inflammation. Nat. Commun. 13, 7535 (2022).
69. O. H. Munz, S. Sela, B. S. Baker, C. E. Griffiths, A. V. Powles, L. Fry, Evidence for the presence of bacteria in the blood of psoriasis patients. Arch. Dermatol. Res. 302, 495–498 (2010).
70. P. Weisenseel, J. C. Prinz, Incidental detection of S. pyogenes-DNA in psoriatic skin by PCR. Arch. Dermatol. Res. 296, 573–576 (2005).
71. K. Wolk, E. Witte, E. Wallace, W. D. Docke, S. Kunz, K. Asadullah, H. D. Volk, W. Sterry, R. Sabat, IL-22 regulates the expression of genes responsible for antimicrobial defense, cellular differentiation, and mobility in keratinocytes: A potential role in psoriasis. Eur. J. Immunol. 36, 1309–1323 (2006).
72. D. Gutowska-Owsiak, A. L. Schaupp, M. Salimi, S. Taylor, G. S. Ogg, Interleukin-22 downregulates filaggrin expression and affects expression of profilaggrin processing enzymes. Br. J. Dermatol. 165, 492–498 (2011).
73. A. K. Ryborg, B. Gron, K. Kragballe, Increased lysophosphatidylcholine content in lesional psoriatic skin. Br. J. Dermatol. 133, 398–402 (1995).
74. T. Sano, D. Baker, T. Virag, A. Wada, Y. Yatomi, T. Kobayashi, Y. Igarashi, G. Tigyi, Multiple mechanisms linked to platelet activation result in lysophosphatidic acid and sphingosine 1-phosphate generation in blood. J. Biol. Chem. 277, 21197–21206 (2002).
75. J. Aoki, A. Taira, Y. Takanezawa, Y. Kishi, K. Hama, T. Kishimoto, K. Mizuno, K. Saku, R. Taguchi, H. Arai, Serum lysophosphatidic acid is produced through diverse phospholipase pathways. J. Biol. Chem. 277, 48737–48744 (2002).
76. C. F. Urban, S. Lourido, A. Zychlinsky, How do microbes evade neutrophil killing? Cell. Microbiol. 8, 1687–1696 (2006).
77. R. M. Kuhn, D. Haussler, W. J. Kent, The UCSC genome browser and associated tools. Brief. Bioinform. 14, 144–161 (2013).
78. D. Karolchik, A. S. Hinrichs, T. S. Furey, K. M. Roskin, C. W. Sugnet, D. Haussler, W. J. Kent, The UCSC Table Browser data retrieval tool. Nucleic Acids Res. 32, D493–D496 (2004).
79. C. Moosmann, T. R. Muller, D. H. Busch, K. Schober, Orthotopic T-cell receptor replacement in primary human T cells using CRISPR-Cas9-mediated homology-directed repair. STAR Protoc. 3, 101031 (2022).
80. C. J. Cohen, Y. F. Li, M. El-Gamil, P. F. Robbins, S. A. Rosenberg, R. A. Morgan, Enhanced antitumor activity of T cells engineered to express T-cell receptors with a second disulfide bond. Cancer Res. 67, 3898–3903 (2007).
81. K. Schober, T. R. Muller, F. Gokmen, S. Grassmann, M. Effenberger, M. Poltorak, C. Stemberger, K. Schumann, T. L. Roth, A. Marson, D. H. Busch, Orthotopic replacement of T-cell receptor α- and β-chains with preservation of near-physiological T-cell function. Nat. Biomed. Eng. 3, 974–984 (2019).
82. J. Ren, X. Liu, C. Fang, S. Jiang, C. H. June, Y. Zhao, Multiplex genome editing to generate universal CAR T cells resistant to PD1 inhibition. Clin. Cancer Res. 23, 2255–2266 (2017)

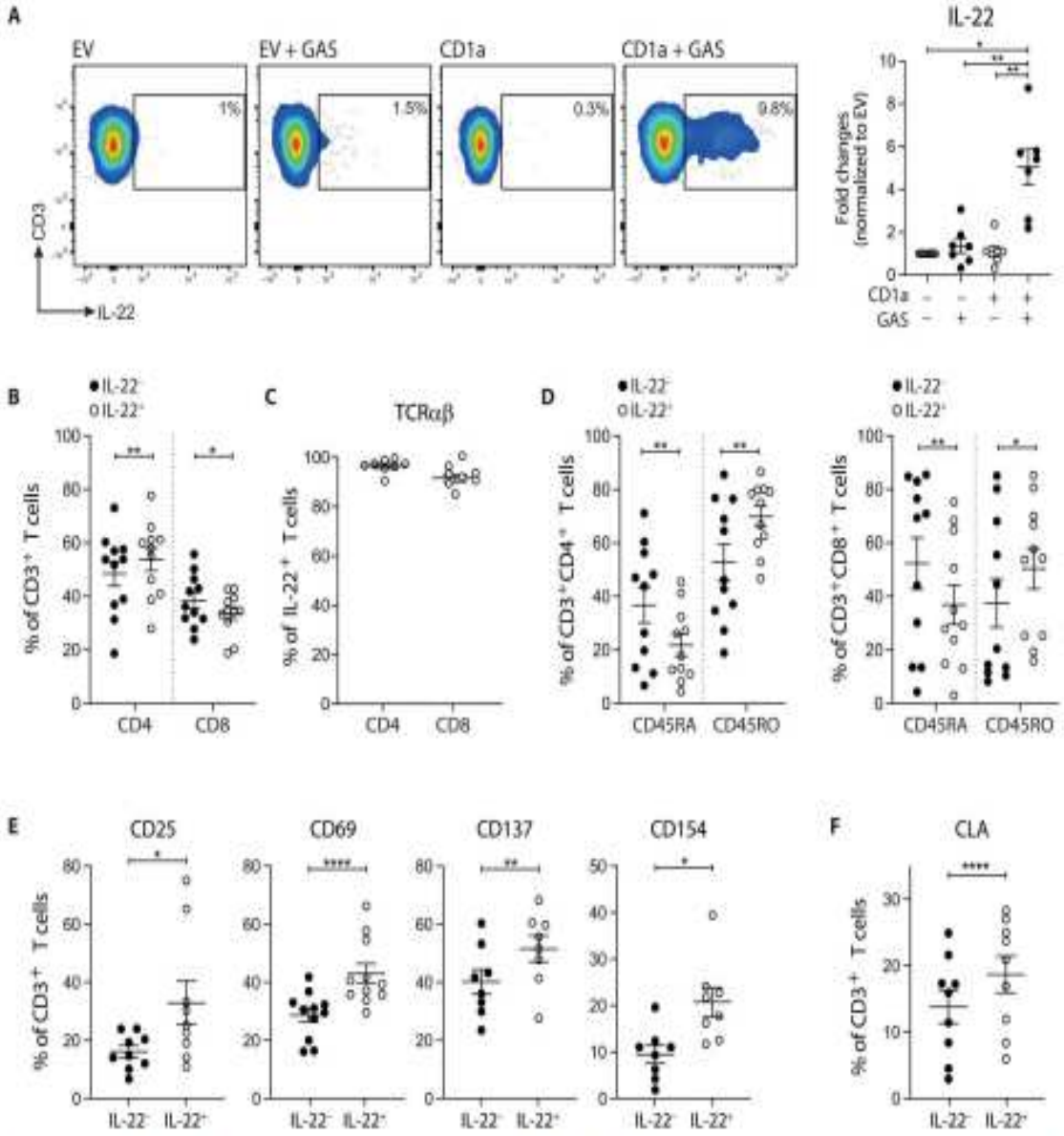

Fig. 1. High frequencies of circulating GAS-responsive CD1a-reactive T cells found in healthy individuals. (**A**) Production of IL-22 from polyclonal blood T cells after 4-hour coculture with control or GAS-infected K562 cells [multiplicity of infection (MOI) = 100] detected by secretion assay. One representative result is shown. Percentages of (**B**) $CD4^+$, $CD8^+$, and (**C**) $TCR\alpha\beta^+$ population in IL-22–secreting GAS-responsive T cells analyzed by flow cytometry. (**D**) Percentages of $CD45RA^+$ and $CD45RO^+$ in IL-22–secreting GAS-responsive $CD4^+$ and $CD8^+$ T cells analyzed by flow cytometry. Expression of (**E**) CD25, CD69, CD137, CD154, and (**F**) CLA on IL-22–secreting GAS-responsive T cells analyzed by flow cytometry. Each symbol represents an individual donor (means ± SEM) ($n = 7$ to 11). $^*P < 0.05$, $^{**}P < 0.01$, and $^{****}P < 0.0001$; repeated-measures (RM) one-way ANOVA with Tukey's post hoc test (A and B) or two-tailed paired t test (D to F). Data are representative of more than three independent experiments.

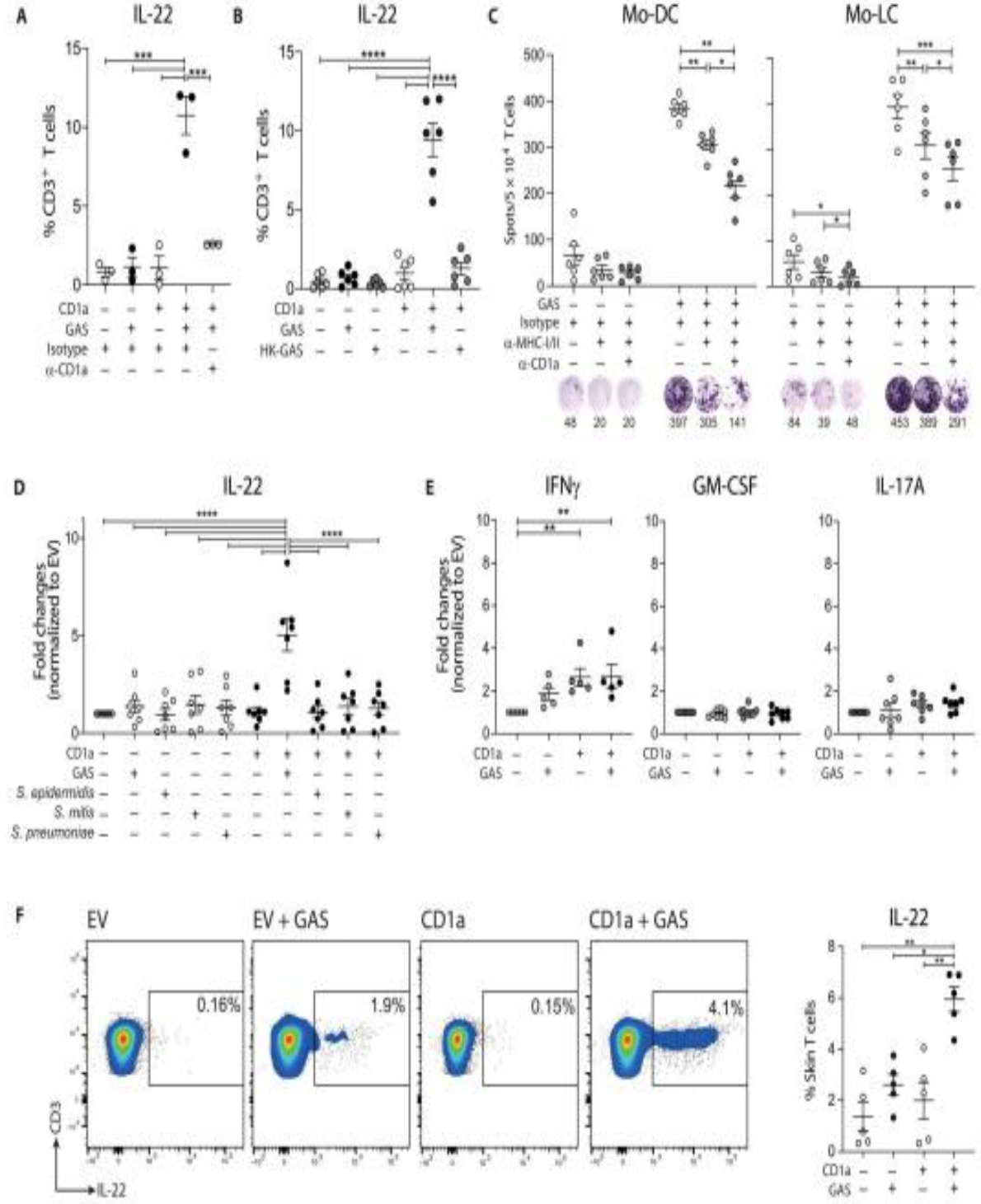

Fig. 2. High frequencies of cutaneous GAS-responsive CD1a-reactive T cells found in healthy individuals. (**A**) Production of IL-22 from polyclonal blood T cells detected by secretion assay after 4-hour coculture with control and GAS-infected K562 cells (MOI = 100) in the presence of anti-CD1a or control IgG (10 μg/ml) ($n = 3$). (**B**) Production of IL-22 from polyclonal blood T cells detected by secretion assay after 4-hour coculture with heat-inactivated GAS-infected K562 cells ($n = 6$). (**C**) Secretion of IL-22 from autologous blood T cells assessed by ELISpot after 16-hour coculture with control or GAS-infected mo-DCs or LC-like cells (MOI = 20) in the presence of anti-CD1a or control IgG (10 μg/ml). Anti–HLA-A,B,C (10 μg/ml) and HLA-DR (10 μg/ml) were added to block peptide-specific T cell response. One representative result is shown of three independent experiments ($n = 6$). (**D**) Production of IL-22 from polyclonal blood T cells detected by secretion assay after 4-hour coculture with control, GAS-, *S. epidermidis*–, *S. mitis*–, and *S. pneumoniae*–infected K562 cells (MOI = 50) ($n = 7$). (**E**) Production of IFN-γ, GM-CSF, and IL-17A from polyclonal T cells detected by secretion assay after 4-hour coculture with control or GAS-infected K562 cells (MOI = 50) ($n = 5$ to 8). (**F**) Production of IL-22 from polyclonal skin T cells after 4-hour coculture with control or GAS-infected K562 cells (MOI = 50) detected by secretion assay. One representative result is shown ($n = 5$). Each symbol represents an individual donor (means ± SEM). *$P < 0.05$, **$P < 0.01$, ***$P < 0.001$, and ****$P < 0.0001$; two-way ANOVA with Tukey's post hoc test (A to D) and RM one-way ANOVA with Tukey's post hoc test (E and F). Data are representative of three or more independent experiments.

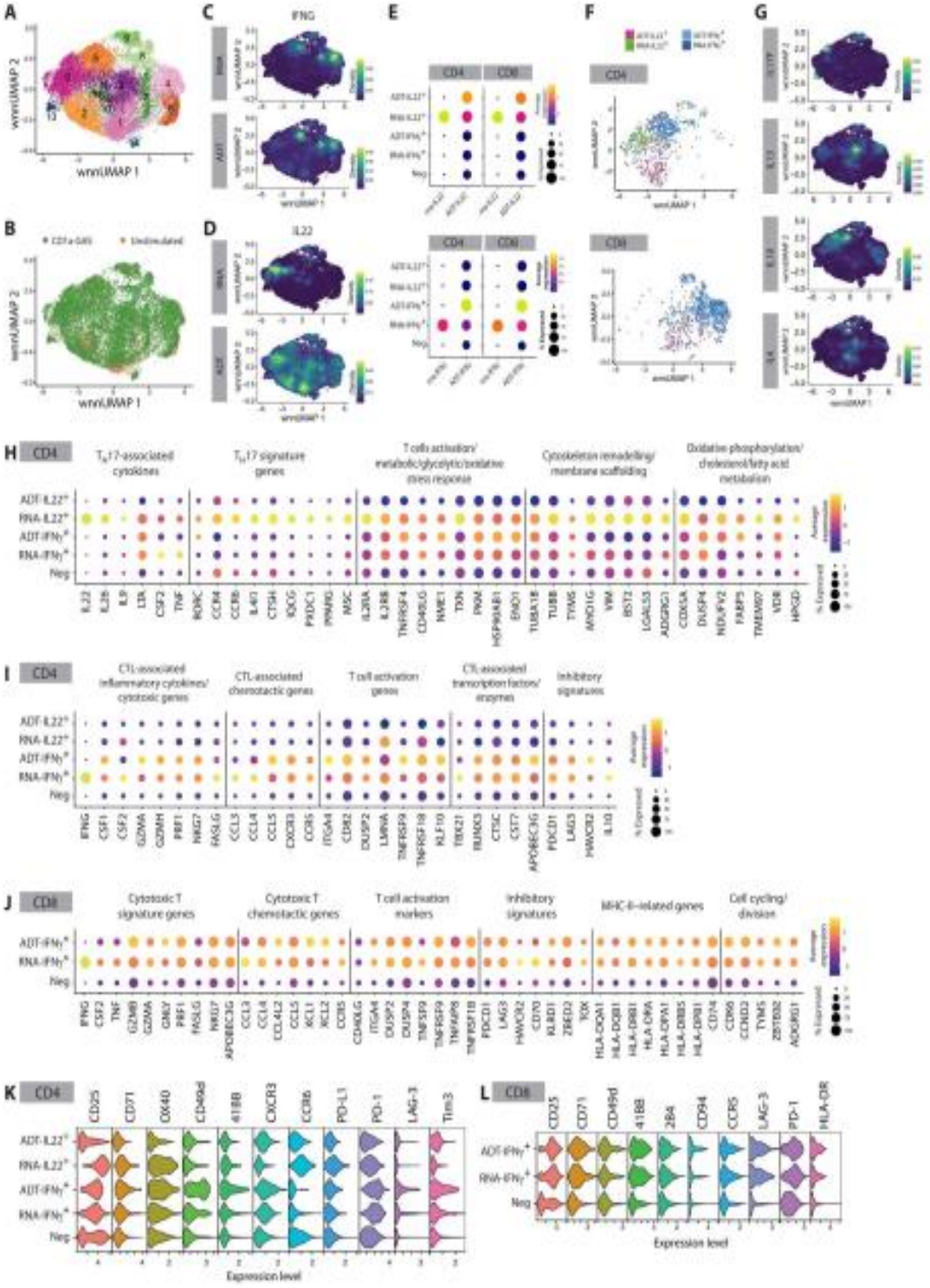

Fig. 3. scRNA-seq reveals diverse functionalities of the IL-22– and IFN-γ–secreting CD1a-reactive GAS-responsive T cells. Single-cell multiomic analysis of skin CD3$^+$ cells after 6-hour coculture with GAS-infected K562-CD1a cells (MOI = 50). (**A**) UMAP plot showing unbiased clustering of the skin CD3$^+$ cells. (**B**) UMAP plot with cell clusters identified on the basis of the coculture conditions [GAS-infected K562-CD1a (n = 4) versus unstimulated control (n = 2)]. Nebulosa plots showing mRNA and protein expression density of IFN-γ (**C**) and IL-22 (**D**) from skin CD3$^+$ cells. (**E**) Dot plots showing the gene expression signatures of IL-22 or IFN-γ mRNA and protein (ADT) level of the ADT–IL-22$^+$, RNA–IL-22$^+$, ADT-IFN-γ$^+$, RNA–IFN-γ$^+$, and IL-22$^-$IFN-γ$^-$ (Neg) skin T cells. (**F**) UMAP plot showing the clustering relation of the CD4$^+$ and CD8$^+$ ADT–IL-22$^+$, RNA–IL-22$^+$, ADT–IFN-γ$^+$, and RNA–IFN-γ$^+$ skin T cells. (**G**) Nebulosa plots showing gene expression density of *IL-17F*, *IL-13*, *IL-10*, and *IL-4* from skin CD3$^+$ cells. Dot plots showing the gene expression signatures of IL-22–producing skin CD4$^+$ T cells (**H**), IFN-γ–producing skin CD4$^+$ T cells (**I**), and IFN-γ–producing skin CD8$^+$ T cells (**J**). Violin plots showing the surface marker expressions (ADT) signatures of IL-22– and IFN-γ–producing skin CD4$^+$ T cells (**K**) and IFN-γ–producing skin CD8$^+$ T cells (**L**).

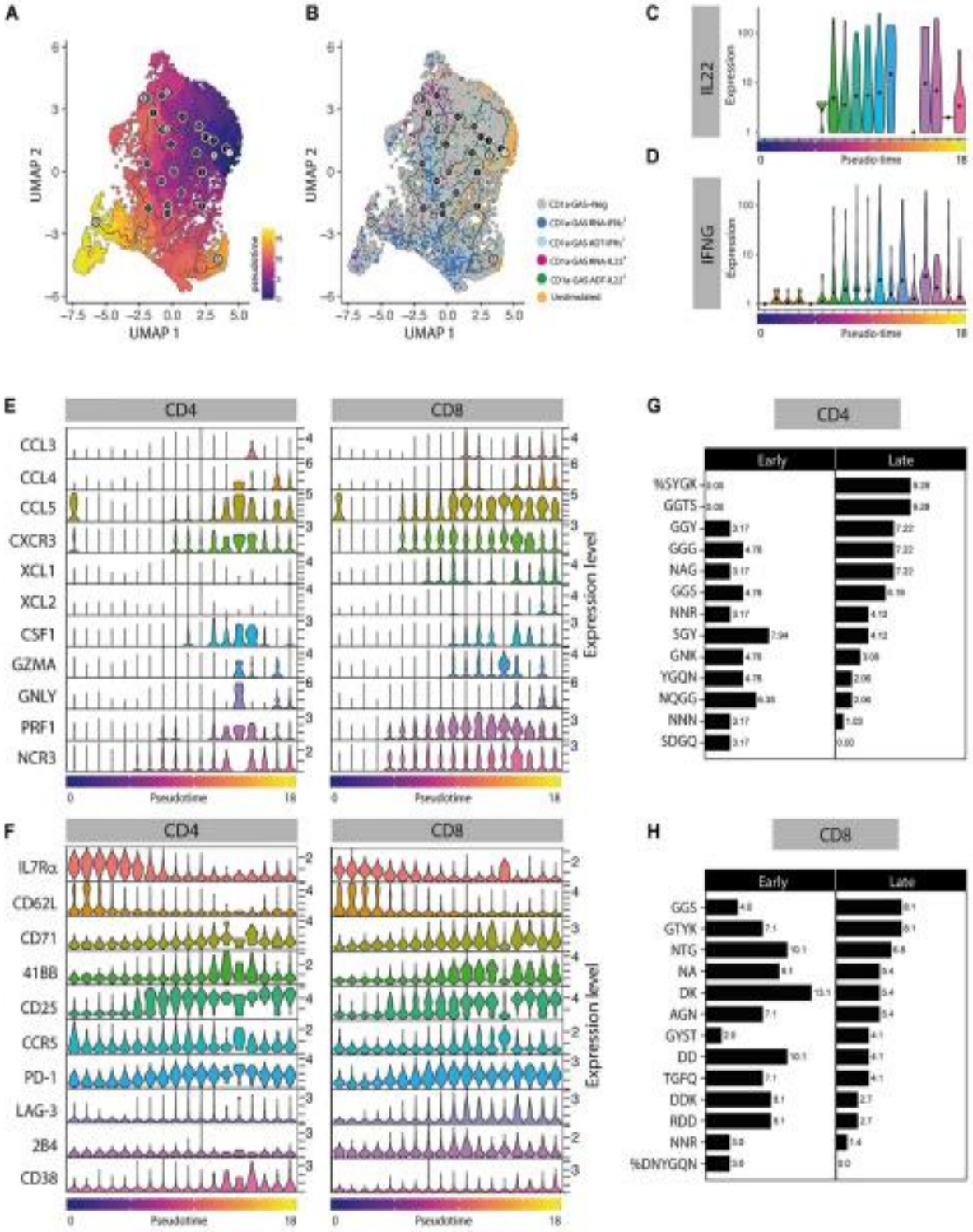

Fig. 4. Pseudo-time trajectory analysis depicts an effector gradient of skin T cells in response to CD1a presentation. (**A**) Trajectory visualization of skin CD3$^+$ cells after 6-hour coculture with GAS-infected K562-CD1a cells (MOI = 50). Cells were ordered and colored according to their pseudo-time on UMAP plot. (**B**) UMAP plot capturing pseudo-time progression of skin CD3$^+$ cells by cytokine production. Violin plots showing IL-22 (**C**) and IFN-γ (**D**) mRNA expression level changed over pseudo-time trajectory. Violin plots demonstrating selective DEG (**E**) and surface protein (**F**) expression patterns of the indicated markers in skin CD4$^+$ and CD8$^+$ T cells changed over pseudo-time trajectory in response to CD1a-GAS presentation (genes with fold change ≥0.5, adjusted $P < 0.05$). Representative motif enrichment of CDR3a from CD4$^+$ (**G**) and CD8$^+$ (**H**) cells located at early and late pseudo-time. The percentage of clonotypes containing each motif is indicated.

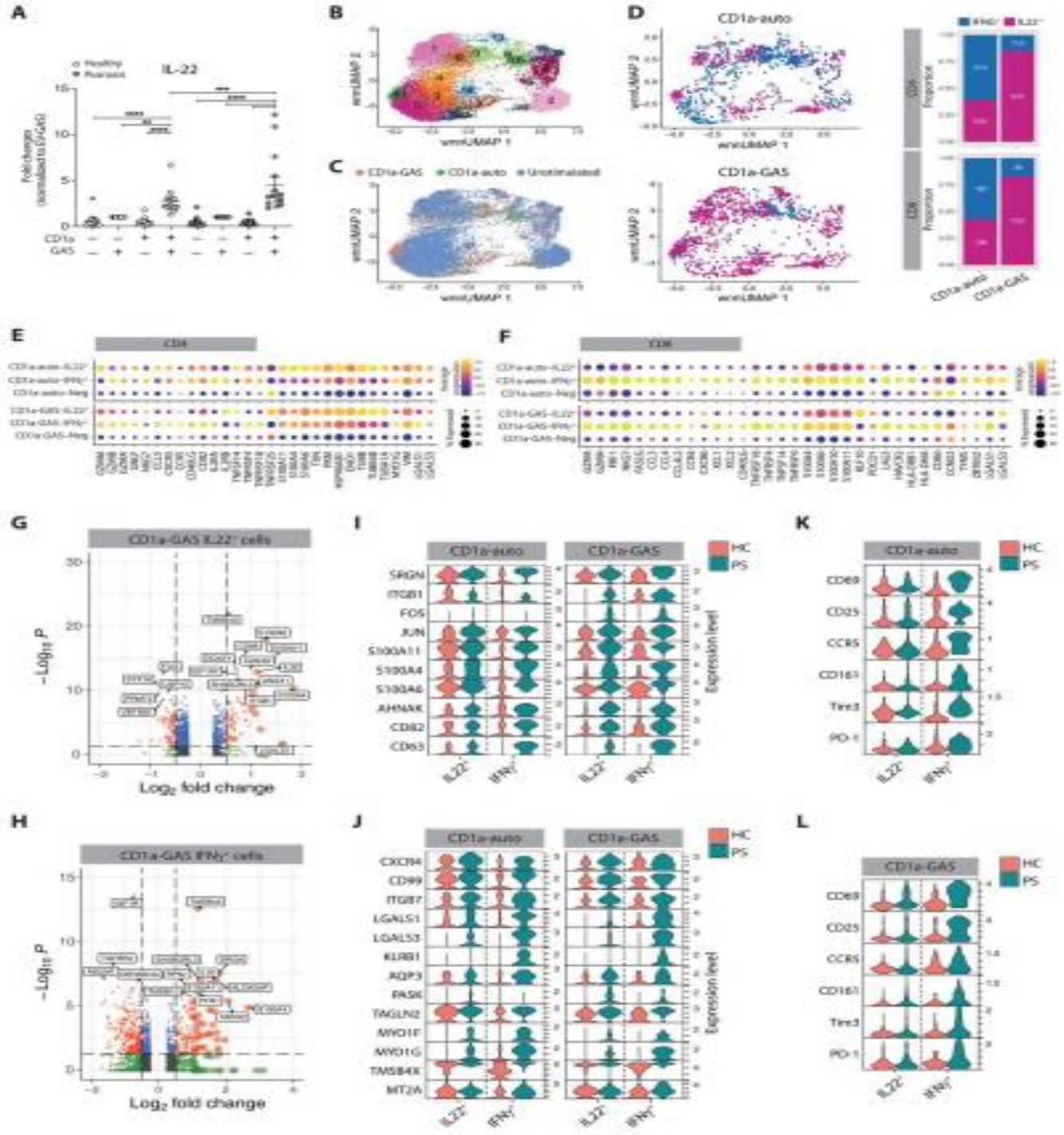

Fig. 5. Psoriatic blood T cells show hyperreactivity in response to CD1arelated presentation. (A) Production of IL-22 from healthy (n = 15) or psoriatic (n = 15) polyclonal blood T cells detected by secretion assay after 4-hour coculture with control or GAS-infected K562 cells (MOI = 50). Each symbol represents an individual (means ± SEM). **P < 0.01, ***P < 0.001, and ****P < 0.0001; two-way ANOVA with Tukey's post hoc test. Data are representative of more than three independent experiments. (B to L) Single-cell multiomic analysis of blood CD3+ cells isolated from five healthy and three individuals with PS (psoriasis) after 6-hour coculture with unpulsed K562-CD1a (CD1a-auto) or GAS-infected K562-CD1a cells (CD1aGAS). (B) UMAP plots showing unbiased clustering of the blood CD3+ cells. (C) UMAP plots showing the clustering of blood CD3+ cells according to the treatments (CD1a-auto, CD1a-GAS, and unstimulated). (D) UMAP plots showing the clustering of IFN-γ and IL-22–secreting cells (left) and their relative proportion within each coculture condition (right). Dot plots showing the gene expression signatures of IL-22– and IFN-γ– producing blood CD4+ (E) and CD8+ (F) T cells of healthy donors from CD1a-auto and CD1a-GAS treatments (selective genes with fold change ≥0.5, adjusted P < 0.05). Volcano plots showing DEGs in IL-22– (G) and IFN-γ–producing (H) psoriatic CD4+ T cells, comparing with their healthy counterparts. The red symbols in volcano plots represent significantly up-regulated or down-regulated genes (fold change ≥0.5, adjusted P < 0.05). Only genes with ±0.25 log2 fold changes are shown on the volcano plots. Violin plots demonstrate selective DEGs (I and J) and surface proteins (K and L) between psoriatic and healthy IL22– and IFN-γ–producing blood CD4+ T cells with indicated coculture conditions (genes or proteins with fold change ≥0.5, adjusted P < 0.05).

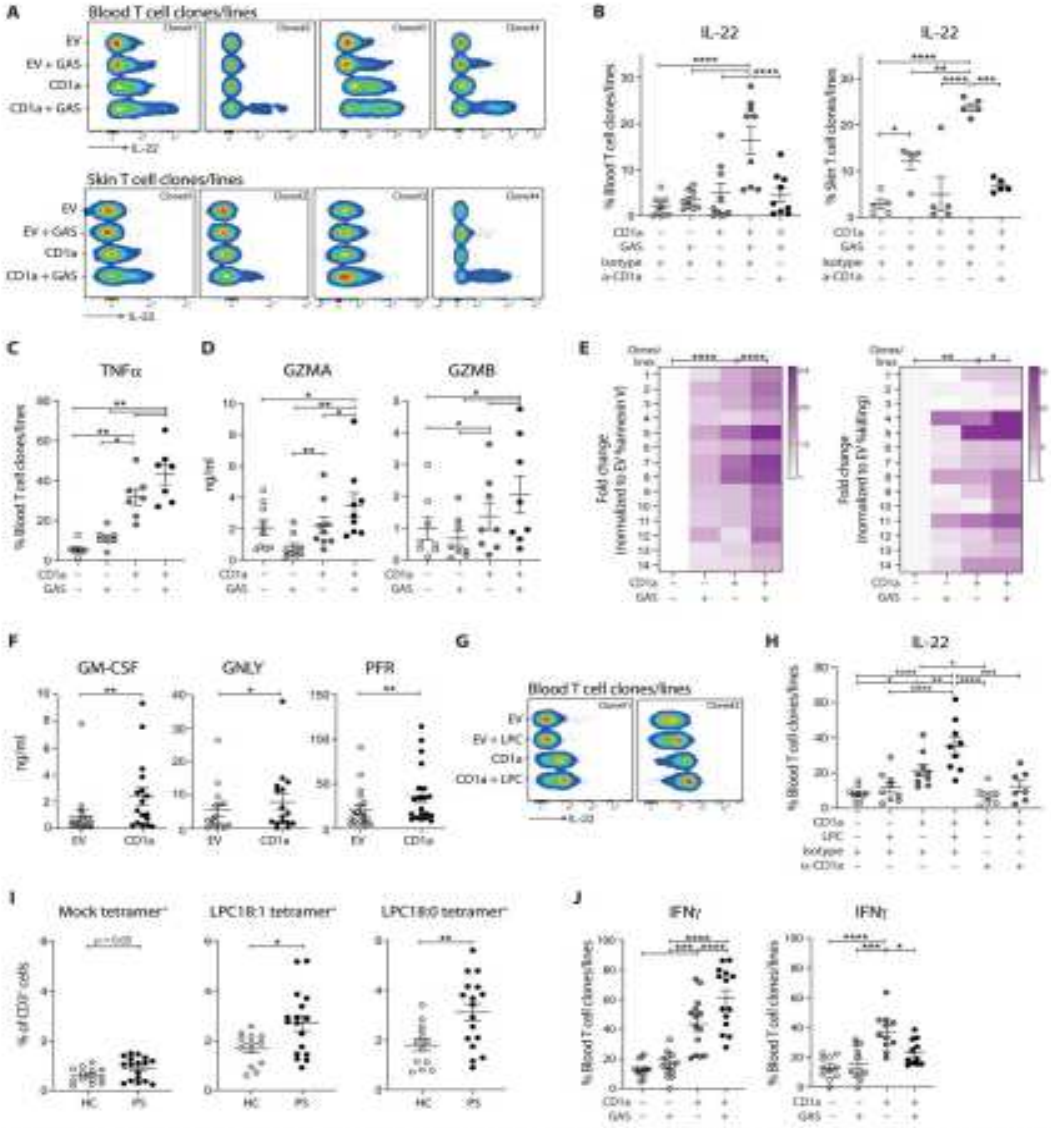

Fig. 6. GAS drives the clonal expansion and activation of CD1a-reactive T cells with the ability to lyse CD1a-expressing infected target cells. (**A** and **B**) Production of IL-22 from expanded blood or skin CD1a-reactive T cell clones/lines detected by secretion assay after 4-hour coculture with control and GAS-infected K562 cells (MOI = 50). Anti-CD1a or isotype-matched control antibody (10 μg/ml) was added to block CD1a-specific activation. Four representative results are shown ($n = 5$ to 9). (**C**) Production of TNF-α from expanded blood CD1a-reactive T cell clones/lines detected by secretion assay after 4-hour coculture with control and GAS-infected K562 cells (MOI = 50) ($n = 7$). (**D**) Secretion of granzyme A and granzyme B from expanded blood CD1a-reactive T cell clones/lines analyzed by bead-based immunoassays after 24-hour coculture with control and GAS-infected K562 cells (MOI = 50) ($n = 8$ or 9). (**E**) Flow cytometry analysis of the killing capacity of the blood $CD8^+$ CD1a-reactive T cell clones/lines. The percentage of apoptotic cells (annexin V^+, left) and the percentage of killing (right) result graph were calculated as the fold change of each condition to the K562-EV ($n = 14$). (**F**) Secretion of GM-CSF, granulysin (GNLY) and perforin (PFR) from expanded blood CD1a-reactive T cell clones/lines analyzed by bead-based immunoassays after 24-hour coculture with control and GAS-infected K562 cells (MOI = 50) ($n = 16$ to 20). (**G** and **H**) Production of IL-22 from expanded blood CD1a-reactive T cell clones/lines detected by secretion assay after 4-hour coculture with control or LPC-pulsed K562 cells (150 μM). Anti-CD1a or isotype-matched control antibody (10 μg/ml) was added to block CD1a-specific activation. Two representative results are shown ($n = 9$). (**I**) CD1a tetramer staining of $CD3^+$ T cells in a cohort of 13 healthy controls and 17 patients with PS. Percentages of indicated $tetramers^+$ cells among all T cells analyzed by flow cytometry are shown. Each symbol represents an individual donor (means ± SEM). (**J**) Production of IFN-γ from expanded blood CD1a-reactive T cell clones/lines detected by secretion assay after 4-hour coculture with control and GAS-infected K562 cells (MOI = 50) ($n = 14$, left; $n = 11$, right). Each symbol represents a T cell clone/line (B, C, D, F, H, and J) (means ± SEM). $^*P < 0.05$, $^{**}P < 0.01$, $^{***}P < 0.001$, and $^{****}P < 0.0001$; two-way ANOVA with Tukey's post hoc test (B and H), RM one-way ANOVA with Tukey's post hoc test (C, D, E, and J) or two-tailed paired *t* test (F and I). Data are representative of more than three independent experiments.

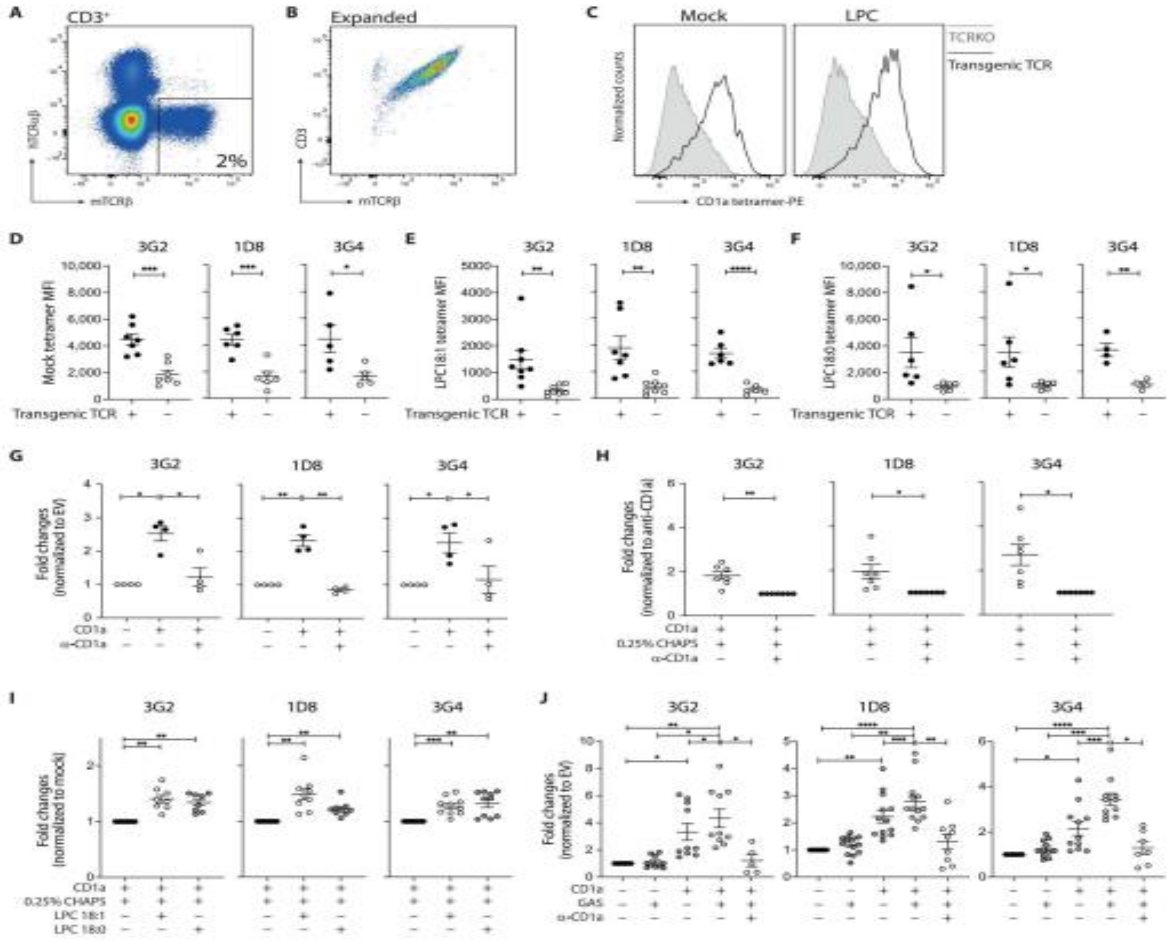

Fig. 7. TCRs derived from GAS-responsive CD1a-autoreactive T cell clones render CD1a-lipid specificity. (A) Representative image showing the successful replacement of the endogenous TCR with transgenic TCR-expressing mouse constant region. (B) Representative image showing the purity of the expanded transgenic TCRexpressing T cells. PBMCsfrom multiple donors were engineered and sorted per target TCR. (C) Representative images of TCR-transgenic T cellsstained with mock-treated or LPC-treated CD1a tetramers. (D to F) Mean fluorescence intensity (MFI) of indicated CD1a tetramer on each TCR-transgenic T cells (n = 4 to 8). (G) Production of intracellular cytokine (IFN-γ– or GM-CSF) from expanded TCR-transgenic T cells analyzed by flow cytometry after 4-hour coculture with K562 cells. Anti-CD1a or isotype-matched control antibody (10 μg/ml) was added to block CD1a-specific activation. The overall data were graphed as the fold change of each condition to the CD1a blockade condition (n = 4). (H) Cytokine (IFN-γ– or GM-CSF) release from TCR-transgenic T cells cocultured with bead-bound CD1a treated with 0.25% CHAPS (mock) measured by intracellular staining and analyzed by flow cytometry after 4-hour coculture. The overall data were graphed as the fold change to the CD1a blockade condition (n = 7). (I) Cytokine (IFN-γ– or GM-CSF) release from TCR-transgenic T cells cocultured with bead-bound CD1a treated with indicated lipids, measured by intracellular staining, and analyzed by flow cytometry after 4-hour coculture. The overall data were graphed asthe fold change to the mock condition (n = 8 to 10). (J) Production of intracellular cytokines(IFN-γ– or GM-CSF) from expanded TCR-transgenic T cells analyzed by flow cytometry after 4-hour coculture with control or GAS-infected K562 cells(n = 10 to 13). Anti-CD1a or isotype-matched control antibody (10 μg/ml) was added to block CD1a-specific activation. Each symbol represents a T cell clone/line (means ± SEM). *P < 0.05, **P < 0.01, ***P < 0.001, and ****P < 0.0001; two-tailed unpaired t test (D to F), two-tailed paired t test (H), RM one-way ANOVA with Tukey's post hoc test (G and I), or mixed-effects one-way ANOVA with Tukey's post hoc test (J). Data are representative of more than three independent experiments.

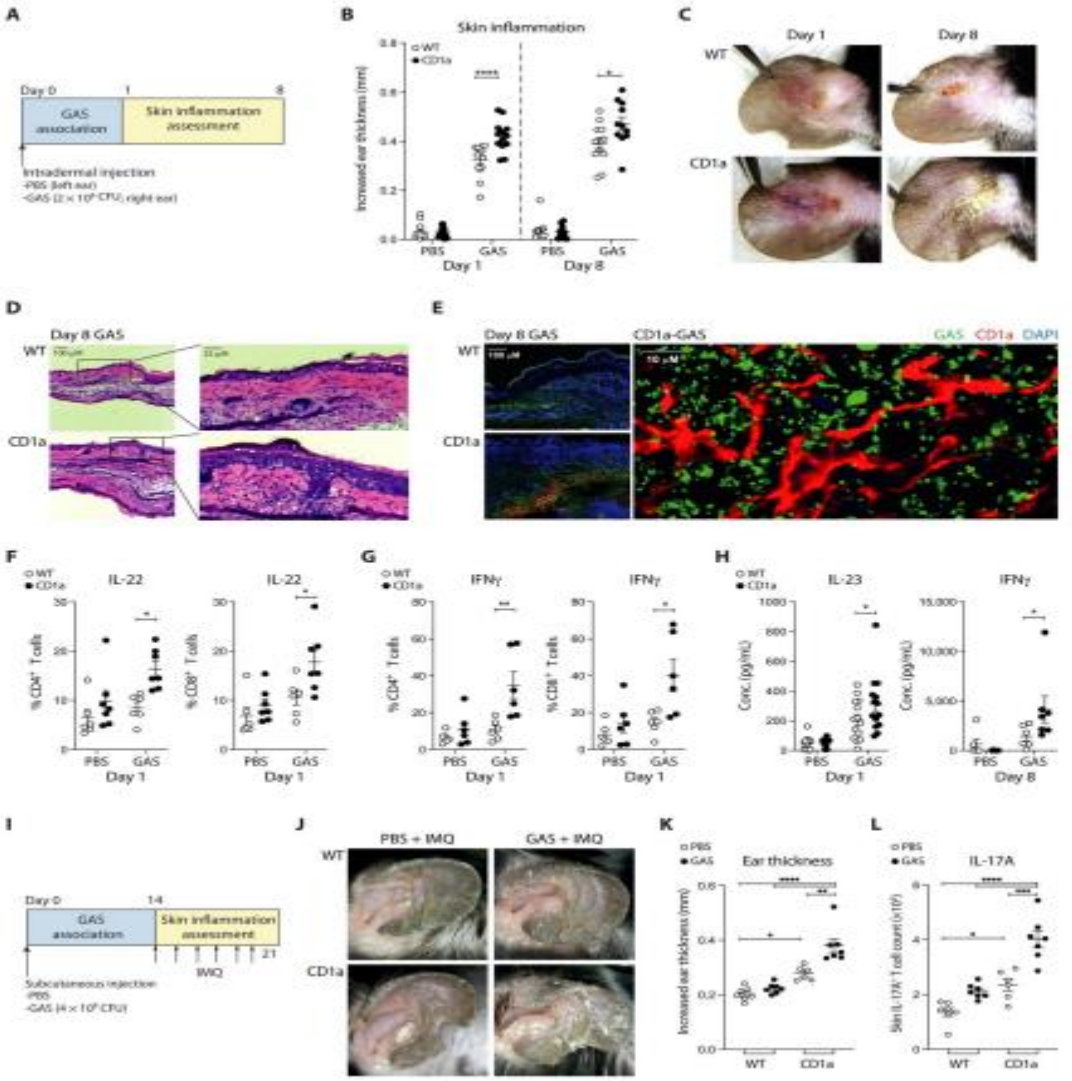

Fig. 8. GAS exacerbates skin inflammation through CD1a in vivo. (A) Schematic of GAS-induced skin inflammation. (B) Measurement of ear swelling induced by GAS infection of WT and CD1a transgenic mice (CD1a) at days 1 and day 8 (n = 12 to 14). (C) Representative images of inflammation on days 1 and 8 of the GAS infection of WT and CD1a transgenic mice. (D) Microscopy of hematoxylin and eosin–stained cross sections of ears from mice infected with GAS for 8 days. (E) CD1a and GAS within ear skin of WT and CD1a transgenic mice 8 days after GAS infection were visualized by immunofluorescence [4′,6-diamidino-2-phenylindole (DAPI) (blue), anti-CD1a (red), and anti-GAS (green)]. (F and G) Intracellular staining analysis of T cell cytokines in draining lymph nodes from mice infected 1 day after GAS infection (n = 6 or 7). (H) Concentrations of IL-23 and IFN-γ in ear skin extracts of GAS-infected WT and CD1a transgenic mice were analyzed by bead-based immunoassays after 1- and 8-day GAS inoculation (n = 6 to 14). (I) Schematic of IMQ-induced skin inflammation after GAS infection. (J) Representative images of psoriasiform inflammation on day 7 of the IMQtreated WT and CD1a transgenic mice with or without prior GAS infection. (K) Day 7 measurement of ear swelling induced by IMQ treatment of WT and CD1a transgenic mice (CD1a) with or without prior exposure of GAS (n = 6 to 7). (L) IL-17A–producing T cell counts per ear by intracellular staining of the IMQ-treated WT and CD1a transgenic mice with or without prior GAS infection (n = 6 or 7). Each symbol represents an individual mouse (means ± SEM). *P < 0.05, **P < 0.01, ***P < 0.001, and ****P < 0.0001; two-way ANOVA with Tukey's post hoc test (B, F, G, K, and L) or two-way ANOVA with Šídák's post hoc test (H). Data are representative of more than three independent experiment